AIR-SEA INTERACTION WITH SSM/I AND ALTIMETER

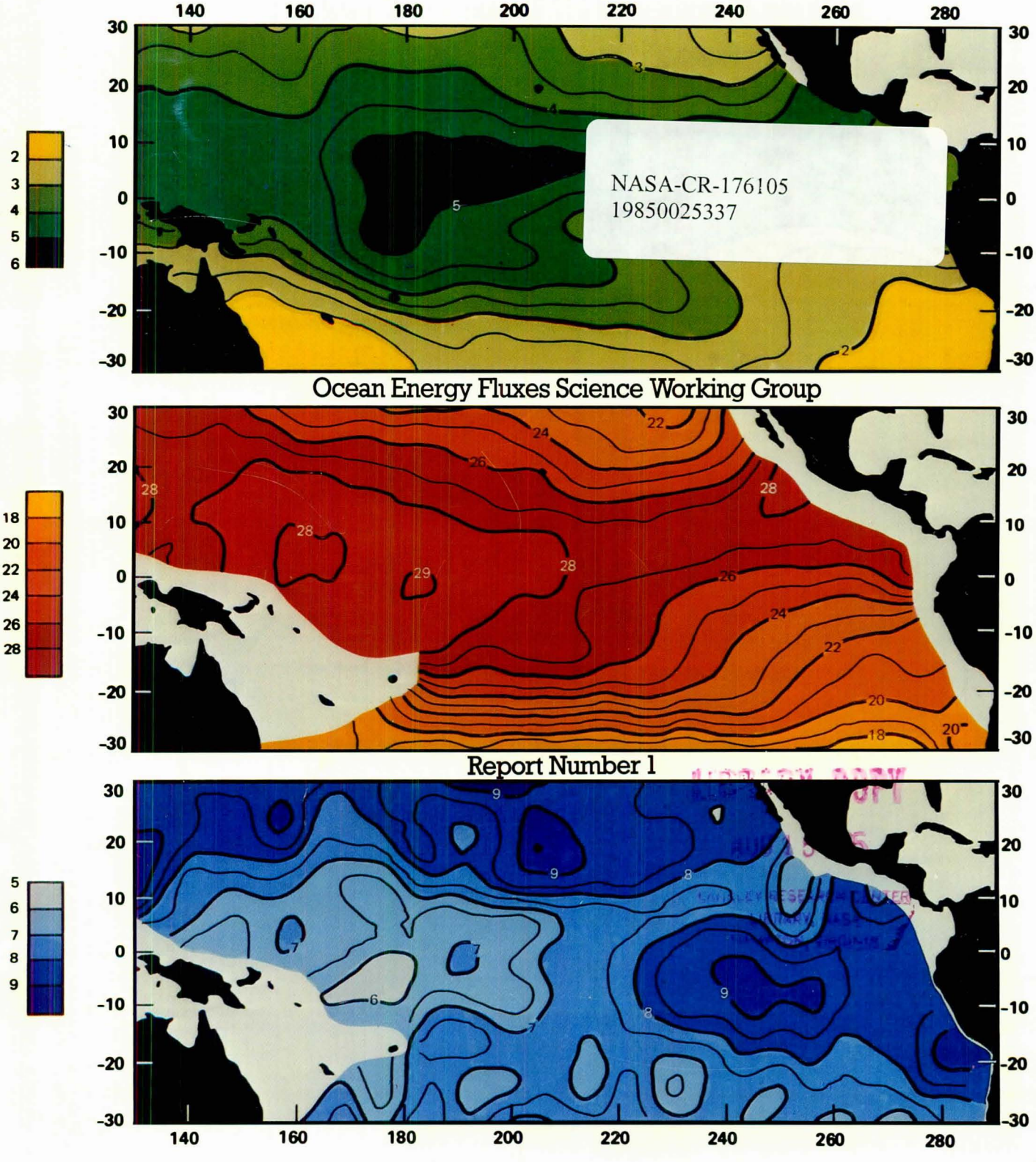

Ocean Energy Fluxes Science Working Group

Report Number 1

AIR-SEA INTERACTION WITH SSM/I AND ALTIMETER

Report of the NASA Ocean Energy Fluxes
Science Working Group

JUNE 1985

The Jet Propulsion Laboratory
California Institute of Technology
Pasadena, California

ABOUT THE COVER:

Average distributions of water vapor (top), sea surface temperature (middle) and wind speed (bottom) in g/cm^2 , $^\circ C$, and m/s, as measured by the NIMBUS/SMMR in the tropical Pacific for the month of October, 1982, during the height of the 1982-83 El Niño. Coastal measurements of wind speed and sea surface temperatures are not available due to land contamination of sensor observations. (Illustration courtesy of Tim Liu, JPL.)

This document was produced under NASA Contract Number JPL956773 to Nova University.

Published by the Nova University/NYIT Press, Fort Lauderdale, Florida, June 1985.

FOREWORD

Looking to the future, NASA's plans for the next decade include the flight of a scatterometer aboard the U.S. Navy Remote Ocean Sensing System (N-ROSS) satellite; a dedicated altimeter mission, the Ocean Topography Experiment (TOPEX), and a color scanner aboard a platform of opportunity. These missions are planned to fly in the early 1990's. In the interim, two satellites scheduled for launch in 1985 and 1986, although not intended specifically for oceanographic applications, have potential for ocean research. The first is the U S. Navy's Geodetic Satellite (GEOSAT), which will carry an altimeter; the second is number one in a series of Defense Meteorological Satellites which will carry a Special Sensor Microwave/Imager (SSM/I).

To assess the useful ocean parameters that can be obtained from GEOSAT and SSM/I data, and to review the scientific problems that can be addressed using these data, the Ocean Energy Flux Working Group was appointed to provide recommendations to NASA. This report presents the results of their study. We express our gratitude to Peter Niiler and the other members of this group for their thoughtful and timely recommendations. It is hoped that the oceanographic utilization of these GEOSAT and SSM/I data will provide both the experience and the understanding necessary to more fully exploit NASA's missions planned for the early 1990's.

William Patzert, Manager
Physical Oceanography Program
NASA Headquarters

TERMS OF REFERENCE

The Ocean Energy Fluxes Science Working Group was established in March 1984 by the Earth Science and Applications Division of NASA. The group was asked:

(a) To identify scientifically useful parameters for air-sea interaction that can be obtained from the DMSP SSM/I sensor (launch: early 1986) and the GEOSAT altimeter (launch: March, 1985);

(b) To review the scientific problems that can be addressed using these parameters;

(c) To assess the status of and needed improvements in algorithms used to transform satellite data to geophysical parameters;

(d) To identify auxiliary data needed to verify and calibrate the necessary algorithms, as well as *in situ* data that would scientifically complement SSM/I and GEOSAT data;

(e) To formulate specifications for processing, archiving, and distributing the data by the Pilot Ocean Data System (PODS) at the Jet Propulsion Laboratory (JPL) or other agencies.

This is a report of the study carried out by the Science Working Group (SWG). The conclusions and recommendations were formulated principally at a meeting held at Scripps Institution of Oceanography, La Jolla, California, during 18–20 April, 1984.

We wish to acknowledge the University of Miami's Remote Sensing Facility personnel, particularly programmer Angel Li, for providing their time, computing facilities, and laser printer during the final production phase of this report. Support for the SWG and report production was provided by NASA Contract JPL956773, through Nova University.

Peter Niiler
SWG Chairman

OCEAN ENERGY FLUXES SCIENCE WORKING GROUP

Peter Niiler, Chairman	Scripps Inst. of Oceanography
Dudley Chelton	Oregon State University
James Cornelius	Fleet Numerical Oceanography Center
Bruce Douglas	NOAA/National Geodetic Survey
Norman Grody	NOAA/National Earth Satellite Service
Jeffrey Hilland	NASA/Jet Propulsion Laboratory
Barry Hinton	University of Wisconsin
James Hollinger	Naval Research Laboratory
David Honhart	U.S. Naval Observatory
Paul Hwang	NASA/Goddard Space Flight Center
Kristina Katsaros	University of Washington
Timothy Liu	NASA/Jet Propulsion Laboratory
Robert Lo	Naval Research Laboratory
Jim L. Mitchell	Naval Ocean Research & Development Activity
Charles Morris	NASA/Jet Propulsion Laboratory
Eni Njoku	NASA/Jet Propulsion Laboratory
Peter Taylor	Institute of Oceanographic Sciences
Frank Wentz	Remote Sensing Systems
Thomas Wilheit	NASA/Goddard Space Flight Center
Janet Witte, Coordinator	Nova University

Contents

1 INTRODUCTION

The air and sea interact in a variety of modes which in the atmosphere on very large scales determine Earth's climate, and on very small scales control the development of intense ocean storms. In the ocean, the energy for circulation is derived entirely from air-sea interaction processes. The communication between these two fluid media is through fluxes of momentum and heat from the air to the ocean and fluxes of heat and moisture from the ocean to the air.

A central scientific problem is to determine the air-sea fluxes accurately so that a clear physical understanding of the interaction process can be achieved. This allows the coupled ocean and atmospheric circulation to be modeled, and in a number of space and time scales allows their joint evolution to be predicted. When weather prediction is to be achieved over successively longer times over continents, influences of increasingly larger ocean areas need to be considered. When climate prediction is considered, knowledge of global air-sea interaction becomes crucial.

In the past three decades, direct measurements have been made of turbulent momentum and heat exchange between the ocean and atmosphere under a wide variety of synoptic weather conditions. Using turbulent, planetary boundary layer theory as a guide, practical formulas for estimating heat and momentum fluxes from synoptic weather observations from ships are now in wide use. For example, estimation of synoptic momentum flux to the ocean requires knowledge of synoptic wind speed and direction, sea state, and the vertical stability of the air boundary layer as expressed by air and sea temperature and humidity differences. The heat flux to the ocean is composed of four components: solar heating, latent flux, long wave flux, and sensible flux. Estimation of the latent flux to the ocean requires knowledge of wind speed, air specific humidity, and sea surface temperature.

Today our knowledge of the global air-sea fluxes is adequate only along heavily traveled merchant ship routes. South of 20°N latitude, the marine observations are sparse. Using ship data alone, the temporal evolution of fluxes between atmosphere and ocean cannot be computed accurately, and our knowledge of the intensity of the evolving air-sea interaction today is inadequate for purposes of predicting both long-term weather and short-term climate in the atmosphere or changes in the large-scale circulation of the oceans.

A number of important developments in satellite remote sensing techniques have occurred recently which offer the possibility of studying over vast areas of the ocean the temporally evolving energy exchange between the ocean and the atmosphere. Commencing in spring of 1985, passive and active microwave sensors that can provide valuable data for scientific utilization will start to become operational on Department of Defense (DOD) missions. The passive microwave radiometer can be used to estimate surface wind speed, total air column humidity, and rain rate. The active radar, or altimeter, senses surface gravity wave height and surface wind speed.

The Defense Meteorological Satellite Program (DMSP) plans to deploy passive microwave radiometers on a continuing basis. The first, termed SSM/I (Mission Sensor Microwave/Imager), is to be launched in early 1986. The U.S. Navy launched an altimeter on the GEOSAT mission in March of 1985; after 18 months, its orbit will be adjusted to provide a meaningful sampling strategy for ocean surface phenomena. The GEOSAT data will be useful for mapping sea level changes that are associated with the movement of strong ocean current systems and their rings and eddies. This use also is described below. The SSM/I data also can be used for mapping sea ice; this utilization is covered by the NASA Scientific Working Group on Sea Ice.

The utilization of SSM/I and GEOSAT data for air-sea interaction studies is addressed below. These missions were not designed for the optimum scientific utilization. The working premise of this SWG is that avenues have been established within NASA and DOD by which scientists can have a strong input as to how the raw data are calibrated and how the geophysical variables are derived for scientific use. This report addresses the science that can be done and how the data are best used for scientific objectives.

2 SCIENTIFIC STUDIES

2.1 Tropical Ocean and Global Atmosphere (TOGA)

In the tropics, the ocean and atmosphere exhibit closely coupled variabilities in circulation, temperature, and rainfall on monthly to yearly time scales. The 1982–83 El Niño was the largest such departure on record from normal seasonal conditions on the Pacific equator. The air-sea interaction process thought most directly responsible for these dramatic shifts of climate are changes of heat transfer from the ocean to the atmosphere and shifts of the wind stress patterns over the tropical ocean. The Intergovernmental Oceanographic Commission (IOC) and the World Meteorological Organization (WMO) have organized a global study of these phenomena. The scientific objectives are the following:

(a) To determine to what extent the time-dependent behavior of the tropical oceans and global atmosphere system is predictable on time scales of months to years, and to understand the mechanisms of this behavior;

(b) To study the feasibility of modeling the coupled ocean-atmosphere system for the purpose of predicting its variations on time scales of months to years,

(c) To provide the scientific background for designing an observing and data transmission system for operational prediction, if this capability is demonstrated by coupled atmosphere-ocean models.

There are numerous requirements that dictate a range of observations of the combined system:

(a) Basic research into key physical processes,

(b) Diagnostic studies,

(c) Model development and verification.

One of the principal components of TOGA is an air-sea flux measurement program aimed at providing a ten-year data set of monthly values of the fluxes of momentum, heat, and moisture across the air-sea interface. These values are required in the earlier stages for driving ocean models and in the later stages for validating coupled atmosphere-ocean models (WCRP, 1984d).

Strong anomalies of heat flux do occur in the tropics. Figure 2.1 shows the latent plus sensible flux difference between December 1972 (an El Niño year) and December 1973 (a post-El Niño year). The signal associated with El Niño events is in excess of 200 w/m^2. Thus, the evolution of the monthly time scale for tropical sea surface temperature, which largely governs the evolution of atmospheric circulation,

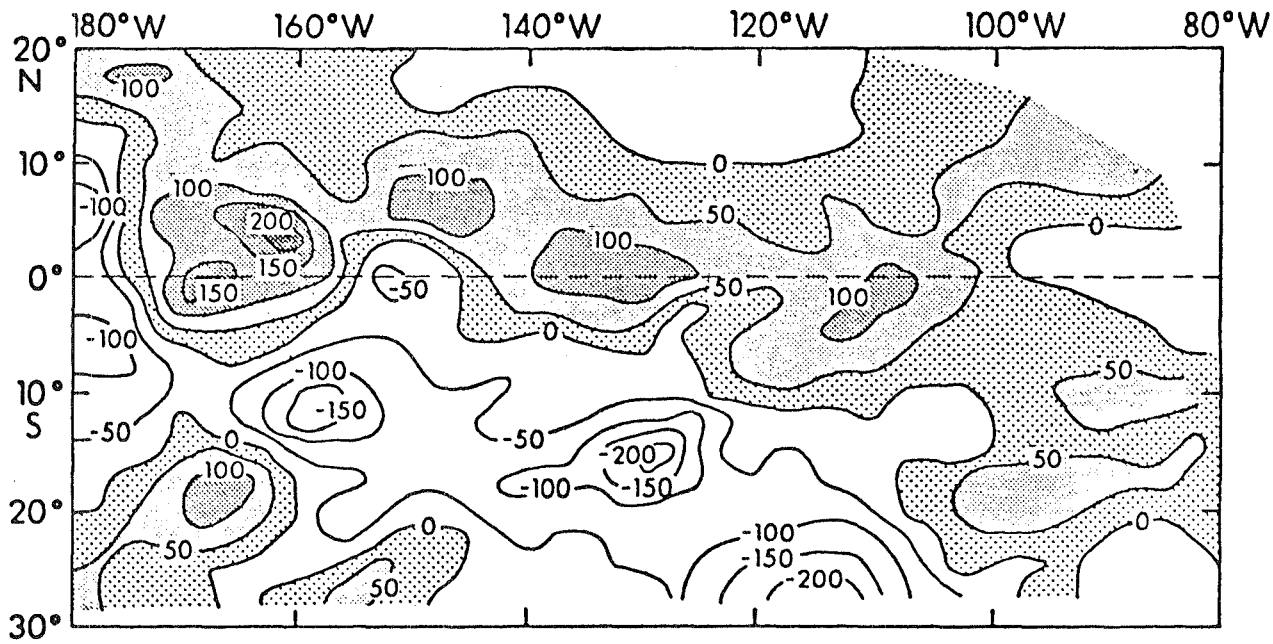

Figure 2.1: The latent plus sensible ocean heat flux difference between December 1972 El Niño and December 1973, non-El Niño. Along the equator the ocean is cooled more and atmosphere is heated more in December 1972 than in December 1973. Contours are in watts per square meter.

is strongly affected by such heat fluxes (McPhaden, 1982; Stevenson and Niiler, 1983; Reed, 1983). Quite simply, if the local monthly excess heat flux of 50–100 w/m^2 over annual mean flux is distributed over the tropical mixed layer having a depth of 50 m, local temperature changes of 0.75–1.50°C can result. Thus to describe as well as to model tropical SST evolution, accurate heat exchange rates are required.

The monthly changes of tropical net heat exchange are determined principally by variations of solar heating and latent cooling (Weare, *et al.*, 1980). As has been widely discussed (*e.g.*, Niiler, 1982), an accuracy of 20 w/m^2 for monthly means and 2°× 2° spatial averages would be sufficient to model or estimate local temperature changes of 50 m deep tropical mixed layers to an accuracy of 0.3°C. Thus a TOGA goal would be a net heat flux estimate of 20 w/m^2 rms accuracy. A useful level is 40 w/m^2 rms accuracy. This would allow modeling or estimation of the seasonal signal and prediction of SST to 0.6°C, which is the accuracy of SST remote sensing or resolution of SST by ships-of-opportunity.

For estimating fluxes by practical formulae, measurements of wind speed and direction, SST, air specific humidity, amount of cloudiness, and speciation are required. In the tropical oceans, sufficient meteorological observations for estimating monthly mean fluxes of heat or momentum exist only along a few shipping lanes. But global remote sensing of air-sea interaction is crucial to the success of the TOGA

objective and must be implemented. The tropical momentum flux determination has been addressed by a TOGA science working group on Interim Ocean Surface Wind Data Sets (WCRP, 1984a). The net surface radiation measurement and SST determination have been addressed by the TOGA science working group on Sea Temperature and Net Surface Radiation Budget (WCRP, 1984b). The conclusions of these studies are that net insolation can be determined with sufficient accuracy for the TOGA goal, and, provided that remote wind speed accuracy can be improved (to 1 m/sec), useful latent heat flux also can be estimated (to 20–40 w/m^2; also see Section 3).

In summary, TOGA objectives and implementation plans require a strong remote sensing program in air-sea heat and momentum fluxes. The parameters that can be derived from SSM/I are crucial to the implementation of the TOGA program. Additionally, global sea level variability from the GEOSAT Exact Repeat Mission (ERM) will play an important role.

2.2 World Ocean Circulation Experiment (WOCE)

The primary goal of WOCE (WCRP, 1984c) is to collect the data necessary to develop and test ocean models useful for predicting climate change. Within this goal, specific aims (WCRP, 1984d) are to determine and understand, on a global basis, the following aspects of the world ocean circulation and their relation to climate:

(a) The large-scale fluxes of heat and fresh water and their divergences on a 5-year mean time scale and, in addition, their annual and interannual variability;

(b) The dynamic balance of the ocean circulation and its response to changing surface fluxes;

(c) Components of ocean variability on months to years, 1000 km to global scales, and the statistics on smaller scales;

(d) The rate and nature of formation, ventilation and circulation of water masses that influence the climate on time scales from 10 to 100 years.

Goal 2 of WOCE is to determine the representativeness of the specific WOCE data sets for the long-term behavior of the ocean, and to find methods for determining long-term changes in the ocean circulation.

Satellite data are considered essential to WOCE. The main field phase is planned for 1990–1995, to run concurrently with the N-ROSS, ERS-1 and TOPEX satellite missions. However, it is stressed that many observational programs need not necessarily be coincident with the main field phase, and that data for Goal 2 are required over a considerably longer time period. Thus relevant data obtained from DMSP and GEOSAT within the runup period and (for later DMSP missions) within the

field phase will be of value to WOCE not only for planning purposes but also for the main scientific research.

The WOCE goals for which DMSP and GEOSAT have the potential to supply useful data are the following:

(a) Large-scale fluxes of heat and water: Determining the vertical flux of heat and water through the sea surface is an important component of this goal. The difficulty of making such a determination has been recognized, and WCRP suggests continued exploration of techniques using total integrated water vapor to estimate latent heat of wide swath satellite measurements for providing the necessary sampling density. The SSM/I on DMSP will be the major source of wide swath integrated water vapor values in the time period 1985–1991. SSM/I wind speed and rain rate data also will be directly relevant to determining the fluxes.

(b) Ocean variability: Altimetric data already have demonstrated their usefulness in ocean variability studies, and GEOSAT altimeter data will be of value in this respect.

2.3 The Ocean Observing System Development Program

The Ocean Observing System Development Program (CCCO, 1984) of the Committee on Climatic Changes and the Ocean (CCCO) was designed to initially provide multi-variable data sets and time series in support of the observational strategy associated with the three streams of the WCRP. Thus the observational requirements of this program are similar to those of TOGA and WOCE. However, there is particular stress on the need to provide a data base for intercomparison with new observational technologies and analysis methods, both to enable thorough evaluation and to preserve continuity with past records. It is expected that the Ocean Observing System will provide the basis of experience from which, as the mechanisms of climate variability and change are better understood, a more cost-effective observing system will be designed and used, on a pilot basis, for climate prediction.

An Ocean Observing System must provide quantitative information on key derived fields, such as wind stress and surface heat flux, on the broad scale needed for validation of numerical models. The potential of DMSP and GEOSAT sensors to provide heat flux information has been discussed elsewhere (see Sections 4.1 and 4.2). The requirement for wind stress information commences before the launch of future scatterometer missions. A workshop on the provision of Interim Ocean Surface Wind Data Sets (WCRP, 1984a) recommended that:

> Operators of satellites with microwave radiometers (*e.g.*, Nimbus 7, DMSP) and altimeters (*e.g.* Geosat) should make provisions to archive

sensor and geophysical data and to make them available to the research community. The sensor and geophysical algorithms should be documented and known errors in the algorithms should be corrected.

2.4 Midlatitude Cyclones

The information on atmospheric water content, as vapor, cloud liquid water, and raindrops, which can be calculated from the SSM/I brightness temperatures, is particularly valuable for the study of midlatitude cyclones. This is true for two reasons. One is obvious: since conventional data are very sparse over the ocean, by producing data for these regions SSM/I is closing a large existing data gap. Secondly, since storms over the oceans are not modified (strongly at least) by terrain variations and strong temperature gradients along the surface, the way in which cyclones evolve when they have minimal external influences may be studied. This is not to say that variations in the drag coefficient and sea surface temperature may not be important for storms over the oceans as well, since there the whole system becomes more subtle.

Another important aspect is that SSM/I data will provide maps at 50 km resolution or better in swaths (1,394 km wide) of integrated atmospheric water vapor, integrated cloud liquid water, and rain rate. This is totally new information not obtainable by any other means. Similar information from radar images or radiosonde sequences from coastal stations, islands, or ships has been obtained previously, but not with the coverage of measurements from space. In particular, it is information on the mesoscale of the moisture field in synoptic frontal zones that holds promise for deepening the understanding of these weather systems, and for aiding in the diagnosis and location of fronts. This will in turn improve the predictability of their future development.

Valuable experience on sensing the atmospheric water as vapor and liquid water was gained from previous passive microwave sensors (see Njoku, 1982, for a review). The primary drawback of the older sensors was the crude resolution, 0(150 km), for water vapor. For liquid water and rain rate, much higher resolution is required, since the natural scales of variability for these phenomena are much smaller: 0(10 km) (Hobbs, 1978). Moreover, the problem affects averages, since at high rain rates, >4 mm/hr, the algorithms for rain rate retrieval are nonlinear (Wilheit and Chang, 1980).

The latest passive microwave sensor from which atmospheric water parameters can be obtained, the Scanning Multi-channel Microwave Radiometer (SMMR), which was flown on SEASAT and Nimbus 7 (Gloersen and Barath, 1977), has a better resolution, 0(50 km), for water vapor and cloud liquid water; rain rate can be measured at 27 km resolution for rain rates <4 mm/hr. For cyclones over the oceans, this resolution is becoming closer to being commensurate with the scales

of variability. In midlatitude cyclones, most of the precipitation is in the form of widespread rain. With the SMMR, individual storms can be analyzed and their development followed. Several studies have been carried out to validate the algorithm retrievals of geophysical data (*e.g.*, Katsaros, *et al.*, 1981; Taylor, *et al.*, 1981a; Alishouse, 1983). A variety of new phenomena have been documented (*e.g.*, Hobbs, 1978; Katsaros and Lewis, 1984; McMurdie and Katsaros, 1985; Matejka, 1980; Taylor, *et al.*, 1981b).

Research topics on midlatitude cyclonic storms can be addressed with the following features of data from SSM/I:

(a) Mesoscale structure of the frontal boundaries between the cold and warm air, which can be seen in all three of the parameters on atmospheric water: total vapor, total cloud water, and rain rate;

(b) Rain band orientation and distribution, which can be seen in the high-resolution data;

(c) The relationship of relative magnitudes of total water vapor, cloud liquid water, and rain rate to storm dynamics, particularly to vertical velocities;

(d) The relationship of total water in a storm, as seen with passive microwave sensors, to precipitation on the coast, *i.e.*, flood hazards and river runoff;

(e) Comparison of life histories of oceanic cyclones in all seasons as they cross the different oceans. The differences in size and sea surface temperature distribution of the oceans may have an influence on the storms' development;

(f) The dramatically developing polar lows, which can be studied particularly well from polar orbiting passive microwave sensors because of the high frequency of sampling at high latitudes.

2.5 Planned and Proposed Studies of Ocean Circulation Involving the GEOSAT Missions

2.5.1 Gulf Stream Regional Energetics Experiment

The Northwest Atlantic Regional Energetics Experiment (REX) being carried out by the Naval Ocean Research and Development Activity (NORDA) will be the first concurrent application of satellite altimetry, regional eddy-resolving numerical modeling, and an extensive field program focused upon an understanding of Gulf Stream mesoscale dynamics and energetics (Mitchell, *et al.*, 1985). The specific scientific issues to be addressed are

(a) What is the relative importance of the barotropic mode (to be uniquely determined by a combination of altimetry and bottom-moored Inverted Echo Sounders with Pressure Gauges (IES/PG)) in determining the dynamics of the Gulf Stream in the region of the New England Seamount chain?

(b) How are fluctuating space and time scales modified by flow through the New England Seamount Chain?

(c) How are fluctuating vertical structure and horizontal exchanges influenced by interaction with strong bathymetry?

Ongoing numerical modeling (Hurlburt and Thompson, 1984) indicates that many of the characteristic scales and phenomena (*e.g.*, stream bifurcation) associated with Gulf Stream fluctuations arise as a result of the relative importance of the barotropic mode and, in many cases, the subsequent interaction with the strong bathymetry of the New England Seamount Chain. One consequence of this interaction is a greatly enhanced frequency of warm core ring generation over the seamounts themselves. Determination of sea level topography from GEOSAT altimetry (see Section 4.2) in the vicinity of seamounts will be dependent upon the extent to which the geoidal effects of the seamounts can be removed

A major objective of the supporting field program is to provide absolute sea level measurements. The calibration for the satellite altimeter in two regions will be studied. The first region is centered on the mean axis of the Gulf Stream at approximately 65–66°N (upstream of the New England Seamount Chain). The second region, centered on approximately 59°W, 39°N, lies immediately downstream of the seamounts. IES/PG's will be deployed over these two regions. Supported by periodic regional CTD and AXBT surveys, the moored arrays will allow for computation of both free surface topography and main thermocline undulation from *in situ* data (Watts and Wimbush, 1981). Use of the IES/PG thus allows separation of the barotropic mode from low-order baroclinic modes. Error budgets associated with the use of IES/PG data for calibration of the altimeter in an absolute sense will be assessed. Absolute calibration of the altimeter range measurement would result in diminished residual orbit error and subsequent increase in the spatial scale over which the altimetry may be applied.

GEOSAT was launched in March, 1985. The initial IES/PG cruise is scheduled for May, 1985, during which the deployment of instruments and a supporting CTD survey are planned. Recovery of the moored instruments is planned for late spring, 1986. Subsequent redeployment and possible augmentation of the instruments is scheduled for summer/fall, 1986, at about the time of the beginning of the GEOSAT-ERM. Numerical model studies and data assimilation experiments are planned throughout the period Additionally, global altimeter crossover point statistics will be used to compile unclassified statistics on global mesoscale variability throughout the nominal GEOSAT and GEOSAT-ERM missions.

2.5.2 Equatorial Pacific Sea Surface Topography Experiment

NOAA/NGS (National Geodetic Survey) is proposing to study large spatial scale fluctuations of sea level with GEOSAT-ERM data. The occurrence of the El Niño/Southern Oscillation (ENSO) in the equatorial Pacific Ocean is related to climate and weather in the United States. This phenomenon is characterized by a weakening or reversal of the western Pacific trade winds, intense warming of equatorial surface waters, and major anomalies in global atmospheric circulation patterns (also see Section 2.1). Collapse of the trade winds causes water to surge eastward across the Pacific basin, changing sea level by 20–30 cm.

At present there is only fragmentary information on how this redistribution of water occurs, but detailed patterns of sea level change can be mapped with a satellite altimeter. Furthermore, a search can be conducted for similar occurrences in other oceans. This project will use GEOSAT altimeter data to form global mean sea surfaces in order to monitor the large-scale change of dynamic height that is associated with events such as ENSO. Work will be coordinated with the U.S. TOGA program.

Global GEOSAT altimeter data are required in order to apply algorithms to correct the ephemeris of the satellite. Tide, EM bias, and propagation corrections also will be applied to the data. The unclassified release of data from the geodetic portion of the GEOSAT mission is not adequate for this project because the data sets close to the SEASAT tracks will occur too infrequently in time and will be broken into relatively short segments. The data analysis will be carried out at a secure facility to provide the proper protection for the GEOSAT altimeter data and ephemerides. The product of this project will be data sets showing the change of sea surface height in the tropical Pacific from Southeast Asia to Central/South America at regular intervals for the duration of the GEOSAT mission. Since only changes in sea surface topography are to be reported, no gravity or geoid signatures will be revealed. This program will be greatly enhanced with topographic variability available from the GEOSAT-ERM.

2.5.3 Gulf of Mexico Dynamic Topography and Circulation

The Gulf of Mexico is an ideal basin for testing ocean circulation models and their ability to assimilate new data types. Because of the Gulf's limited size and well defined inflow and outflow through the Yucatan and Florida Straits, it is possible to envision experiments for studying the circulation of the Gulf as a whole. NOAA/NGS is proposing to conduct a survey of the Gulf using a long-range aircraft equipped with AXBT's, radar altimeter, and a Global Positioning System (GPS) geodetic receiver for precise positioning relative to another GPS receiver on land. The AXBT data can be used to construct the surface dynamic topography, while the altimeter and GPS systems will provide the total sea surface height. The

difference between these two surfaces is, to a good approximation, the geoid. Once the geoid has been determined, subsequent GEOSAT altimeter profiles can be used to derive maps of dynamic topography and thus the surface circulation of the Gulf of Mexico.

All GEOSAT altimeter data in the Gulf of Mexico are required along with the precise ephemeris computed from Doppler tracking data. Data processing and analysis will be carried out at a secure facility to preserve the integrity of the classified data and ephemeris. The product will consist of a series of maps of the Gulf of Mexico showing dynamic topography and surface circulation.

2.5.4 Three-year Global Ocean Mesoscale Variability

GEOS 3 and SEASAT demonstrated the potential of altimetry for mapping the mesoscale eddy field, but neither provided the global long-term description desired. GEOSAT, and particularly the GEOSAT-ERM, will make an important contribution in this area. It is proposed to derive global eddy statistics from either crossover (ground track intersections) or collinear differences. The preferred technique will depend on the phase of the GEOSAT mission. Neither technique requires any geoid knowledge. The global altimeter data set is required. Corrections must be made for ocean tides, path length effects, EM bias, sea state, and ephemeris errors. It will be necessary to use the entire data set in order to get an adequate temporal sample. NOAA/NGS will need to generate cross-over statistics, because the algorithm selected to reduce the error of the precise ephemeris from the altimeter data can affect the results. The product of this investigation will be a report containing maps of eddy energy and sea height variability of the global ocean. This product is independent of the marine geoid and gravity, because it is determined from differences of altimeter measurements which contain no gravity or geoid signature.

2.6 Satellite Altimeter Data and Wave Research

The impact of satellite data on ocean wave research has been assessed by Carter and Challenor (1984). They suggest that three major areas of impact will be short- and long-term wave statistics and ocean wave modeling.

For short-term statistics, initial research will be driven by the need to understand the relationships between the sea surface and the altimeter return. This will involve the extension of much ocean wave theory from one to two dimensions and further development of nonlinear theories. The altimeter may provide measurements of important sea state parameters, such as the variance of the vertical acceleration of the sea surface, which are not available from conventional buoy measurements. Such data can be used to derive a wave period (Challenor and Srokosz, 1984). Current research (Srokosz, 1985, unpublished manuscript) suggests that an algorithm giving

joint estimates of significant wave height, skewness, and a parameter possibly related to long-crestedness is derivable. Skewness is expected to be higher in regions of active wind-wave generation and may allow these regions to be distinguished from those where the significant wave height is dominated by propagating swell. The results also would allow a better estimate of the sea state "bias" in altimeter measurements of the mean sea level. For research into the above topics, the altimeter waveform data would be required.

For long-term statistics, altimeters will enable large-scale spatial processes to be studied and, over a number of years, will provide data on which to construct a wave climate model for areas of the world where there are no data now. It will be possible to study the spatial correlation scale and the spatial homogeneity of ocean waves, and hence the spatial variability of wave climate. For these studies, significant wave height data from the satellite are a minimum requirement; however, interpretation may be hindered considerably if the satellite is in a non-repeat orbit.

Although work has commenced on the incorporation of satellite measurements into ocean-wide wave models, Carter and Challenor (1984) suggest that the altimeter will have a relatively small impact compared with scatterometers. However, the altimeter might provide useful significant wave height data for the verification of models; the altimeter wind estimates, being collocated with the H_s values, also may be useful for this purpose. A further use of the combined altimeter wind and wave data may be for the estimation of a swell-related parameter (Guymer, *et al.*, 1985).

Under the International Oceanographic Data Exchange (IODE) system of the IOC, Responsible National Oceanographic Data Centers (RNODC's) are charged with the cataloguing, archiving, and dissemination of certain categories of data. The Marine Information and Advisory Service (MIAS) of the Institute of Oceanographic Sciences (Wormley, England) is the RNODC for instrumentally measured wave data on a world-wide basis, including those data provided by satellites. MIAS receives on average 350 to 370 enquiries per year for wave data (Jones and Tabor, 1984).

3 PARAMETERS AND REQUIRED ACCURACIES

Both of the sensors addressed in this report, the altimeter on GEOSAT and the SSM/I on DMSP, have the potential of measuring ocean surface wind speed. This parameter is required for determining the latent heat flux and available kinetic energy flux to the ocean. Wind speed is required in bulk formulas of heat transfer computation. The kinetic energy provides mechanical stirring of the upper ocean and facilitates transport of heat and salt. There are a number of studies on the portion of the available kinetic energy actually transferred from the atmosphere to the ocean mixed layer (*e.g.*, Denman and Miyake, 1973; Richman and Garrett, 1977); it is proportional to the wind speed cubed. Global coverage of this function south of 20°N cannot be acquired adequately over any time scale with the existing sparse surface data sets.

The SSM/I also will measure the columnar water vapor (precipitable water) W in the atmosphere. Liu and Niiler (1984) have demonstrated that monthly mean W can be related to monthly mean surface layer humidity. Together with wind speed and sea surface temperature measured by spaceborne sensors, monthly mean latent heat flux (evaporation) can be determined over the globe or over an ocean basin (Liu, 1984). Evaporation affects ocean salinity and atmospheric water budget in that it changes the fresh water content of both the upper ocean and the lower atmosphere. For a net water budget, rain rate must be known. The problems of measuring sea surface temperature from space have been addressed in other workshops (*cf.*, JPL, 1984; WCRP, 1984b), and the present accuracies over most of the globe are sufficient for latent heat flux estimation to about ± 20 w/m^2. This section covers in detail the requirements for wind speed and surface layer humidity. Rain rate is discussed in Section 4.1.3, but since rain data are sparse over the ocean, rain determination will require special research programs for the duration of the mission discussed here.

For studies of interannual variability, monthly mean values of the variables will suffice. Current knowledge of the fluxes and related parameters comes mainly from meteorological reports of merchant ships and fishing vessels that are concentrated along shipping lanes and coastal fishing grounds. The sampling density required to evaluate the evolving monthly means depends on the temporal and spatial gradients. Luther and Harrison (1984) found that 21 samples per month are required to produce over 0.90% correlation between sub-sample and true wind stress time series at four island stations representing different wind regimes in the central and western tropical Pacific. The requirement is less stringent at locations with relatively higher annual and interannual energy. Weare and Strub (1981) suggested that more than 11 samples per month for a 5° by 5° area are required to reduce satisfactorily the sampling bias at two coastal regions in the eastern tropical Pacific. At higher latitudes, Fissel, *et al.* (1977) found that sampling once every two days is required to define heat and momentum fluxes at Ocean Weather Station P (50°N), and Taylor (1984) suggested that sampling at a period of 30 hours is necessary to define la-

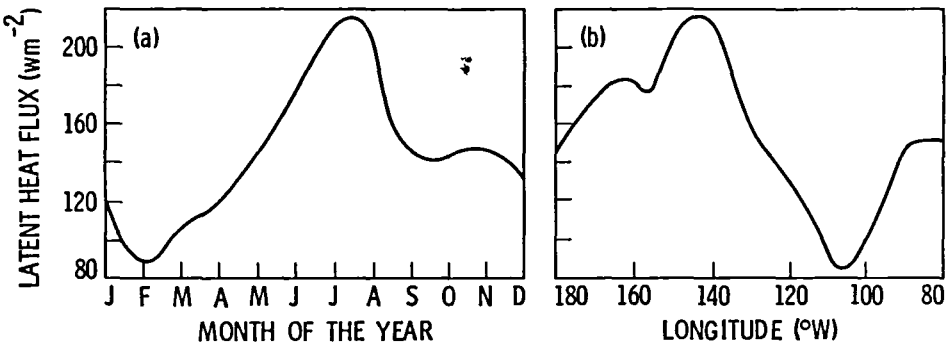

Figure 3.1: Temporal and spatial variations of latent heat flux in the equatorial Pacific, estimated from 20-year monthly means of Weare, *et al.* (1980).

tent heat flux to 20% of the mean during the Joint Air-Sea Interaction Experiment (JASIN) in the North Atlantic. It appears that a sampling rate of once every 1 to 3 days is necessary for much of the ocean.

To estimate the required accuracy for spaceborne sensors, the magnitude of the signal to be measured must be known. Niiler (1982) derived the heat flux difference between the December of a normal year (1973) and the December of an anomalous year (1972) in the tropical Pacific from the data of Ramage, *et al.* (1980). He found that the difference can be as large as 200 w/m^2 (see Figure 2.1). Figure 3.1 shows the temporal and spatial variation of latent heat flux at the equator in the Pacific (Liu, 1984), derived from the 20-year means of Weare, *et al.* (1980). Figure 3.1a shows the annual variation at 135°W on the equator, and Figure 3.1b shows the spatial variation on the equator for August. The monthly mean can exceed 200 w/m^2; the temporal and spatial variations have about the same magnitude: 120 w/m^2. In tropical oceans, the mean and variation appear to have similar magnitudes, and 20% of the variation exceeds 20 w/m^2. For the CAGE Experiment (Dobson, 1983), the required accuracy is 10 w/m^2, corresponding to 20% of the heat flux required to balance the meridional heat transport across 24°N in the North Atlantic. This is compatible with the requirement for monitoring interannual variation in the North Atlantic.

The latent heat flux is generally determined from ship reports by the bulk formula:

$$E = \rho L C_E U (Q_s - Q) \tag{1}$$

where ρ is the surface air density, L is the latent heat of vaporization, C_E is the transfer coefficient for moisture, Q_s is the saturation humidity at sea surface temperature, and U and Q are the wind speed and specific humidity at a level in the atmospheric surface layer. Typical wind speed in the tropical Pacific is about 7 m/s, and the typical value for $Q_s - Q$ is about 5 g/Kg. A 20% accuracy requirement for E corresponds to 20% accuracy requirements in U or Q, *i.e.*, 1.4 m/s or 1 g/Kg.

For 7 m/s wind, to achieve an accuracy of 10 w/m^2 in E requires an accuracy of .4 g/Kg in Q.

To obtain Q from satellite observations, Liu and Niiler (1984) show that a universal relation between monthly mean Q and W can be derived. By using a local regression in the tropical Pacific, monthly mean Q can be predicted to an accuracy of .4 g/Kg, and with a global regression, an accuracy of .8 g/Kg can be achieved. Assuming a 7 m/s wind, these accuracies correspond with approximately 10 and 20 w/m^2 in the determination of latent heat flux with (1). Over tropical oceans, an accuracy of 1 g/Kg in Q requires 10 Kg/m^2 in W. The requirements for W become more stringent in subtropical regions but relax again in midlatitudes, reflecting the decrease of the vertical humidity gradient in the troposphere away from the subtropical highs. A 0.4 g/Kg accuracy in Q requires a 4 Kg/m^2 accuracy in W over tropical oceans, but approximately 2 Kg/m^2 on average over the global oceans.

Hellerman and Rosenstein (1983) demonstrated that the largest amount of available kinetic energy is found in the winter westerlies of the North Atlantic and Pacific, in the summer monsoon of the Arabian Sea, and in the winter westerlies of the Antarctic circumpolar current regions: 0.6, 0 5, 0.4, and 0.3 w/m^2, respectively. The available kinetic energy flux K also can be determined from the bulk formula:

$$K = C_D U^3 \tag{2}$$

where C_D is the drag coefficient. A 20% accuracy requirement in K corresponds to a 6.7% requirement in U. For example, measuring K corresponding to a typical wind speed of 7 m/s to 20% accuracy requires that the wind speed measurement be accurate to .5 m/s. The interannual variation over tropical oceans may be just half of this amount and puts a high demand on the accuracy of wind speed measurements.

In summary, to study latent heat flux over tropical oceans, accuracies of 1.4 m/s in U and 10 Kg/m^2 in W are required, but better accuracies are desirable. The demonstrated accuracies of spaceborne sensors on SEASAT are similar to the requirement in U and about an order of magnitude better in W. Satisfying the .4 g/Kg (10 w/m^2) accuracy over global oceans requires pushing the known capability to the limit. The study of interannual variation of kinetic energy flux, however, requires improved technology.

4 SENSORS AND ALGORITHMS

4.1 The SSM/I Mission

SSM/I is a joint Navy/Air Force project. This system was developed by the Hughes Aircraft Company, under the direction of the Navy Space Systems Activity (NSSA) and the Air Force Division. It is to be flown on the DMSP operational spacecraft as an all-weather oceanographic and meteorological sensor (Hollinger and Lo, 1983).

The SSM/I is a seven-channel, four-frequency, linearly polarized, passive microwave radiometric system. The instrument measures atmospheric/ocean surface brightness temperatures at 19.3, 22.2, 37.0, and 85.5 GHz. These data will be processed on an operational basis by the Naval Oceanographic Command and the Air Force Air Weather Service to obtain near real-time global precipitation maps, sea ice morphology, marine surface wind speed, columnar integrated liquid water, and soil moisture percentage.

The instrument consists of an offset parabolic reflector that is fed by a corrugated, broad-band, seven-port horn antenna. The reflector and feed are mounted on a drum that contains the radiometer, digital data subsystem, mechanical subsystem, and power subsystem. The reflector-feed-drum assembly is rotated about the axis of the drum by a coaxially mounted bearing and power transfer assembly (BAPTA). All data, commands, timing and telemetry signals, and power pass through the BAPTA on slip-ring connectors to the rotating assembly.

A small mirror and hot reference absorber are mounted on the BAPTA and do not rotate with the drum assembly. They are positioned off-axis such that they pass between the feed horn and the parabolic reflector, occulting the feed once each scan. The mirror reflects cold sky radiation into the feed, thus serving, along with the hot reference absorber, as calibration references for the SSM/I. This scheme provides an overall absolute calibration that includes the feed horn. Corrections for spillover and antenna pattern effects from the parabolic reflector are incorporated into data processing algorithms.

The radiometers are total power, balanced mixer, superheterodyne type receivers. The exact operating frequencies and radiometric performance characteristics are given in Table 4.1.

Details of the scan geometry are shown in Figure 4.1. The SSM/I rotates once in 1.90 seconds, during which time the satellite advances 12.5 km. The antenna beams are at an angle of 45° to the BAPTA rotational axis, which is normal to the earth's surface. Thus as the antenna rotates, the beams define the surface of a cone and, from the orbital altitude of 833 km, make an angle of incidence of 53.1° at the earth's surface. The scene is viewed over a scan angle of 102.4° centered on the ground track aft of the satellite, resulting in a swath width of 1394 km. The

Table 4.1: SSM/I Performance Characteristics.

Parameter	Radiometric Performance			
Center Freq., GHz	19.35 ± 0.05	22.235 ± 0.05	37.0 ± 0.1	85.5 ± 0.3
Polarization	VERT AND HORIZ	VERT	VERT AND HORIZ	VERT AND HORIZ
If Bandpass, MHz	10 to 250	10 to 250	100 to 1000	100 to 1500
Radiometric Accuracy, K	1.5	1.5	1.5	1.5
ΔT, K	0.8	0.8	0.6	1.1
Dynamic Temp Range, K	375	375	375	375
Effective Fov (3 dB Antenna Beamwidth; Includes Integ Time) Reference, KM	70 x 45	60 x 40	38 x 30	16 x 14
Integration Time, ms	7.95	7.95	7.95	3.89

radiometer outputs are sampled differently on alternate scans. During the scans labeled A in Figure 4.1, each of the five lower-frequency channels is sampled over 64 equal 1.6° intervals, and each of the two 85.5 GHz channels is sampled over 128 equal 0.8° intervals, or approximately every 11 km along the scan. During the alternate type B scans, only the two 85.5 GHz channels are sampled at 128 equal intervals.

Sampling to 12-bit precision is accomplished by the integrate, hold and dump method with an integration period of 7.95 ms for the five lower-frequency channels and 3.89 ms for the two 85.5 GHz channels. Alternate 0.8° intervals are centered on the midpoints of the 1.6° intervals so that samples of all seven channels are collocated with additional 85.5 GHz samples equally spaced between them. Thus the five lower channels are sampled on an approximate 25 km grid along the scan and along the track. The two 85.5 GHz channels are sampled at one-half this spacing, both cross- and along-track.

The hot absorber and cold sky reflector references are both sampled in the same manner as for the scene data, but over total angles of 8.0°, rather than 102.4°, as they occult the feed horn during the remaining portion of the scan.

The DMSP office has adopted the calibration/validation plan for the SSM/I instrument and algorithm proposed by the Navy (Hollinger and Lo, 1985). The plan includes the validation of the calibration algorithm, the antenna pattern correction algorithm, and the environmental parameter retrieval algorithm to ensure quality performance and proper application of data for scientific purposes.

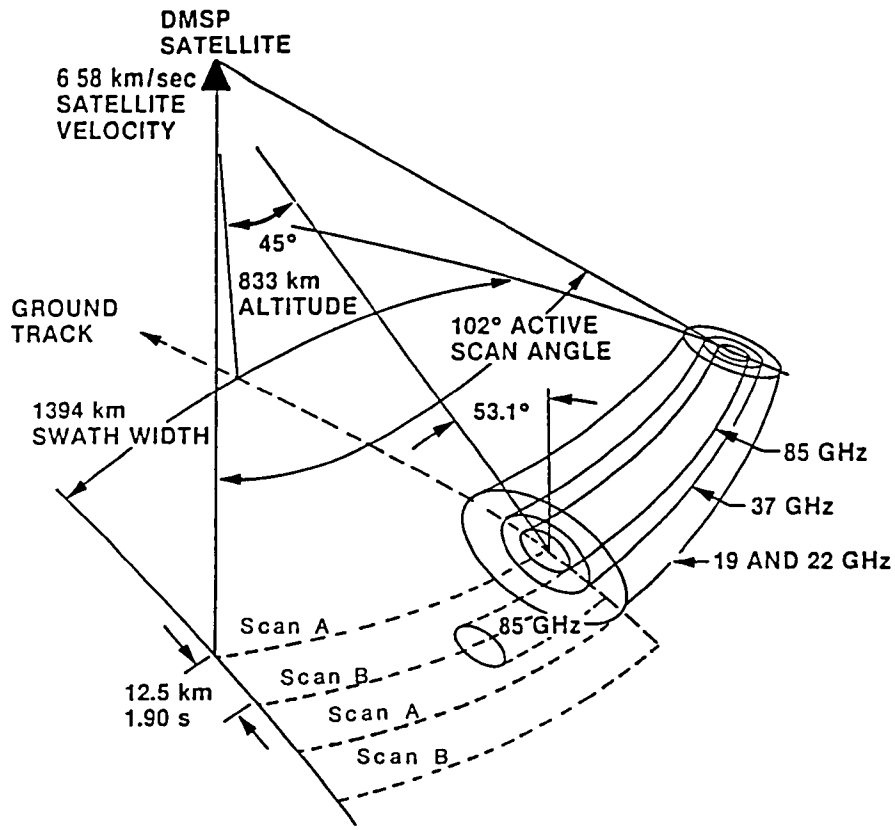

Figure 4.1: SSM/I scan geometry.

4.1.1 The SSM/I Wind Sensing Capability

The potential for SSM/I to measure wind speed over the world's oceans is promising. SSM/I's predecessor, the SSMR, demonstrated a capability to measure wind speed to an accuracy of 2 m/s (Wentz, *et al.*, 1982; Cardone, *et al.*, 1983). However, these SMMR wind speed retrievals relied primarily on the 6.6 and 10.7 GHz channels, which are not present on SSM/I. Since the SSM/I channels are at higher frequencies, which are more subject to atmospheric interference, there is some question as to SSM/I's wind sensing capability. In a recent study (Wentz, *et al.*, 1985) that addresses this question, the SEASAT SMMR higher frequency channels were used to retrieve winds. The results were very encouraging. For 123,000 comparisons over the SEASAT 3-month period, a 1.7 m/s agreement was obtained between the SMMR winds derived from the 21 v-pol and 37 h- and v-pol channels and the SEASAT SASS winds.

Figure 4.2 (from Wentz, *et al.*, 1985) shows SMMR and SASS wind speed comparisons using six different channel combinations for SMMR. The first four combinations are indicative of the earlier SMMR algorithms that relied on the lower frequencies to obtain wind. The last two combinations, which consist of SSM/I channels only, should provide a good indication of the wind sensing capability that will be obtained from SSM/I. As can be seen, there is some degradation in performance in going from the 6.6 and 10.7 GHz systems to the 18 and 37 GHz systems.

The rms difference between the SMMR and SASS winds for the 6.6 and 10.7 GHz systems is about 1.5 m/s, whereas it is 2.2 and 1.7 m/s for the 18 and 37 GHz systems, respectively. Relative to the 37 GHz system, the performance of the 18 GHz system is better at higher winds and worse at lower winds. These results suggest that a four-frequency combination, 18H/21V/37V/37H, may be advantageous for the SSM/I wind retrieval.

It is emphasized that the good agreement between SMMR and SASS winds does not necessarily mean that the actual wind can be measured to a 1 to 2 m/s accuracy. Rather, the SMMR/SASS comparisons indicate that there exists a high correlation between the sea surface roughness characteristics that affect microwave brightness temperatures and radar cross sections. Unfortunately, these intersensor comparisons do not really address the complex boundary layer problem involving the correlation of near-surface winds and sea surface roughness.

Although SSM/I's potential to measure wind looks promising, a number of possible problems do exist. First, there is still considerable debate over the relationship between brightness temperature and wind speed. Furthermore, the uniqueness of the wind dependence can be questioned. Secondary effects such as atmospheric stability and the duration, fetch, and variability of the wind may be significant. Finally, the presence of rain will certainly degrade the wind retrievals. Small rain cells that partially fill a footprint can be mistaken for a heavy uniform cloud layer, and larger rain cells can totally obscure the surface. The SMMR/SASS wind comparisons discussed above considered only 150 km resolution cells, for which the effect of rain is washed out.

4.1.2 The SSM/I Water Vapor Sensing Capability

The ability of microwave radiometers to measure water vapor has been well established for many years. The NIMBUS 5 NEMS (Staelin, *et al.*, 1976), the NIMBUS 6 SCAMS (Grody, *et al.*, 1980), and the SEASAT and NIMBUS 7 SMMR's (Alishouse, 1983; Chang, *et al.*, 1984) all have demonstrated the capability to measure the columnar water vapor content V to within 0 3 to 0.4 g/cm^2 when compared to radiosonde measurements. Much of this small discrepancy between the radiometer and radiosonde water vapor probably is due to the spatial and temporal misregistration between the two instruments. With its 22.235 GHz channel, SSM/I also should provide excellent water vapor information.

The relationship between T_B and V is somewhat nonlinear, with the derivative dT_B/dV decreasing with increasing V. This is particularly true for SSM/I, for which the water vapor channel is at the center (22.235 GHz) of the water vapor absorption line, rather than being offset like SMMR (21 GHz). In the tropics, where the columnar water vapor content can be as high as 6 g/cm^2, this nonlinearity is

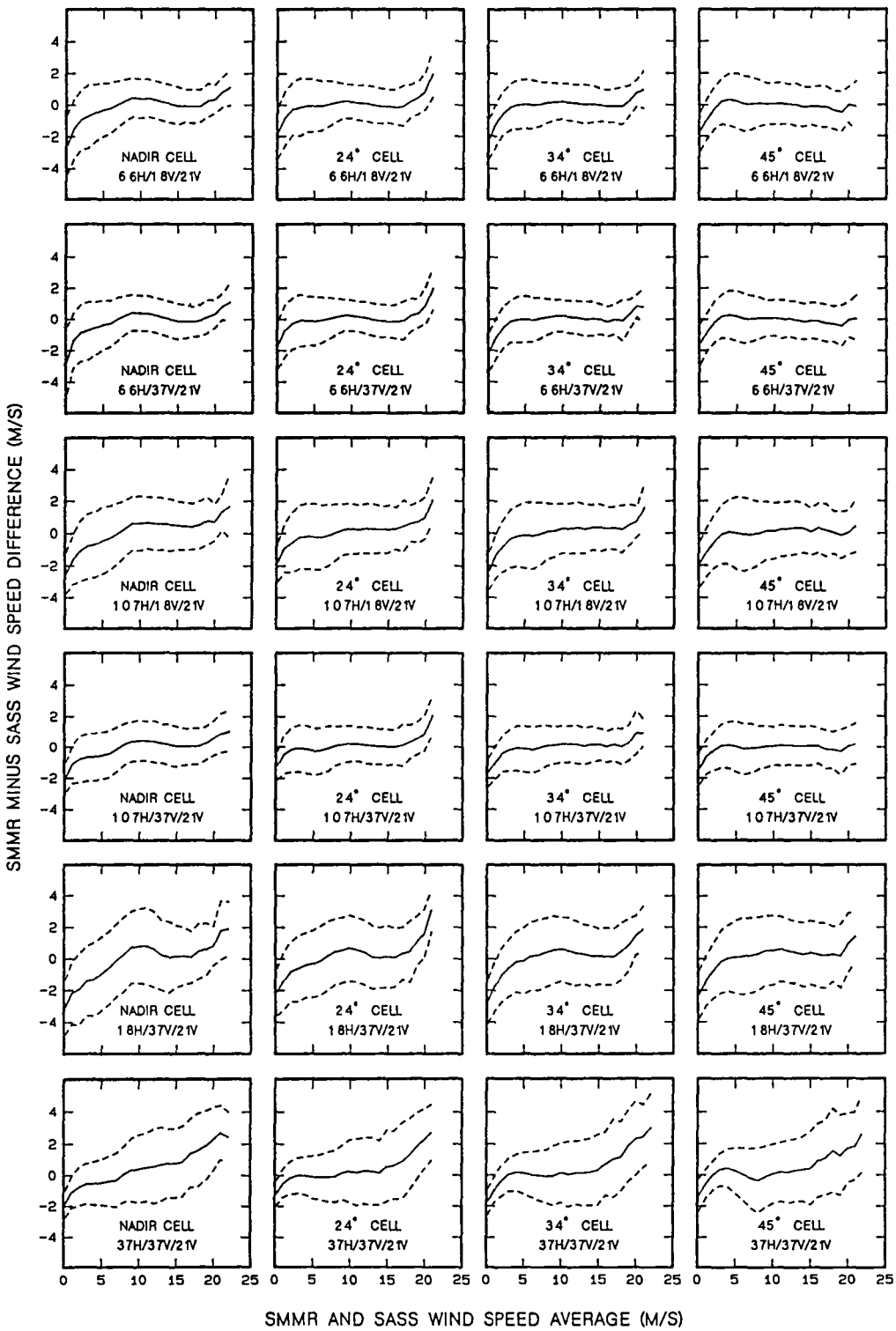

Figure 4.2: A comparison of SMMR and SASS winds at a 150 km resolution for the three-month SEASAT period. For each row of plots the SMMR winds come from a different combination of three SMMR channels. The four plots in a row correspond to different swath positions, going from the satellite subtrack to the outer portion of the swath. The solid curve denotes the mean SMMR minus SASS wind difference, and the dashed curves show the ± 1 standard deviation envelope for the differences.

important and must be taken into account, in order to obtain an unbiased estimate of V.

4.1.3 The SSM/I Precipitation Sensing Capability

The role of precipitation in the dynamics of the earth's ocean-atmosphere system is very important. Unfortunately, precipitation is highly variable in both space and time, making the sampling requirements extremely stringent.

A variety of schemes using visible and infrared observations from both Geostationary (GEO) and Low Earth Orbiting (LEO) satellites have been applied to the precipitation estimation problem (Barrett and Martin, 1981). Recently, microwave observations also have been shown to be useful. They have been directly related to the hydrometeors and thereby represent a new data source for improved satellite observations of precipitation rate. From the microwave measurement, the desired quantity of an integrated rainfall over some period of time can be derived, with a properly designed measurement strategy.

Passive microwave rainfall measurements fall into two regimes: absorption and scattering. Generally at frequencies below the 22 GHz water vapor line, absorption is the dominant process, and at frequencies above the 60 GHz oxygen complex, scattering dominates. Between 22 and 60 GHz, either process can be dominant, depending on the specific situation.

In the absorption regime rainfall is observed through the emission associated with absorption. A cold background is required in order to make such observations, so it is ideally suited for ocean observations. The liquid raindrops themselves are the dominant contributors to this absorption and emission, thereby providing a very direct physical relationship between the rainfall and the observed microwave radiances.

In the scattering regime, the rainfall is observed via the scattering within the rain column, which then reflects the cold cosmic background toward the downward-viewing observer. This process allows the observation of rainfall over any background (Spencer, *et al.*, 1983), but, since the scattering is primarily due to the frozen hydrometeors aloft, the relationship to the rain rate is less direct than in the absorption regime.

Figure 4.3 depicts a model used in relating observed brightness temperatures (radiances) to rain rates. This model has three free significant parameters: freezing level (rain layer thickness), ice layer thickness, and rain rate through the distribution.

If the ice layer is ignored, such a model can be used to generate a set of curves (see Figure 4.4). Displayed here is the calculated brightness temperature over the ocean for a frequency of 19.35 GHz (the frequency of the Nimbus 5 ESMR and the lowest frequency on the SSM/I) as a function of rain rate for 5 different freezing

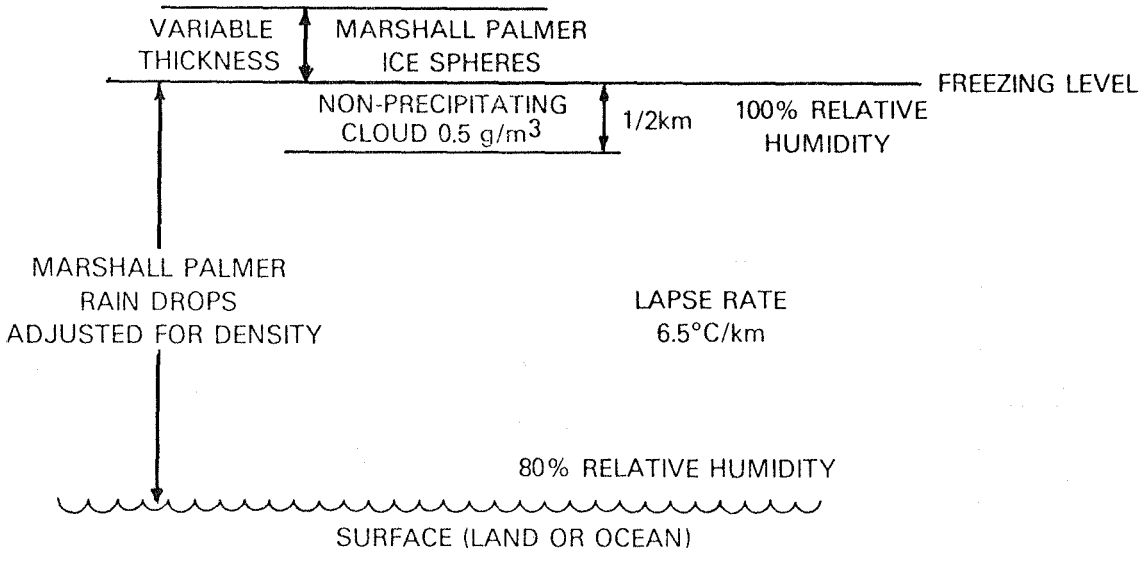

Figure 4.3: A schematic view of the factors entering into the calculation of radiative transfer in precipitation.

level assumptions. For all freezing levels the brightness temperature rises rapidly as a function of rain rate to a maximum in the neighborhood of 20 mm/hr and then merges and drops off slowly with further increases in rain rate. The ignored ice layer is not important at this and lower frequencies but can become quite important at higher frequencies.

This model has been verified both by comparing spaceborne radiometric observations with ground-based radar and by comparing ground-based, upward-viewing observations with direct rain measurements (Wilheit, *et al.*, 1977). Figure 4.5 shows the results of this ground-based validation at 37 GHz. Some freezing level problems have been encountered (see Rao, *et al.*, 1976; Spencer, *et al.*, 1983; Wilheit, *et al.*, 1982).

There are some important open issues. Since rainfall is highly variable in both space and time, this causes a great deal of difficulty for any rain measurement scheme. Moreover, there is in some circumstances a large diurnal cycle in rainfall. This causes a large potential for error in any sun-synchronous measurement approach. If, for the moment, the diurnal component of variability is ignored, some estimates of the statistical component of error in the rainfall estimates based on SSM/I measurements can be arrived at.

The sampling depends on the channel used; here the 85.5 GHz channel, which will have about a 15 km resolution, will be used as an example. The swath width of the instrument will be about 1400 km and the satellite will have a ground speed

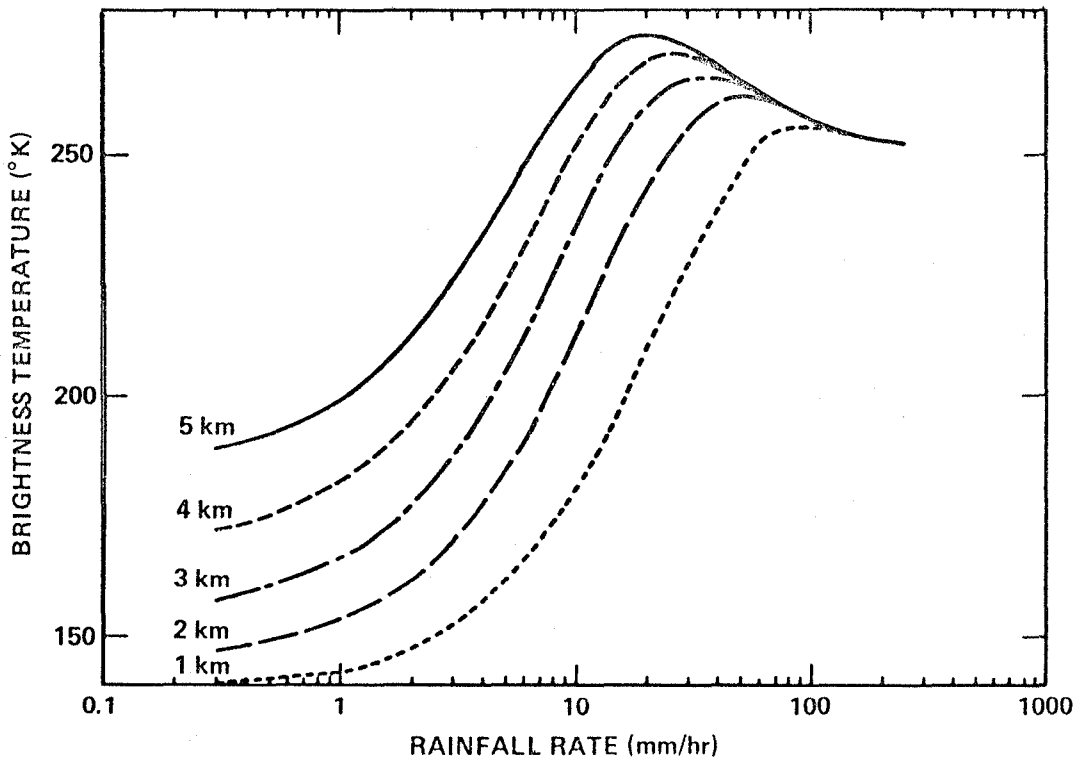

Figure 4.4: Brightness temperature for nadir viewing over an ocean surface at 19.35 GHz for various assumed freezing levels.

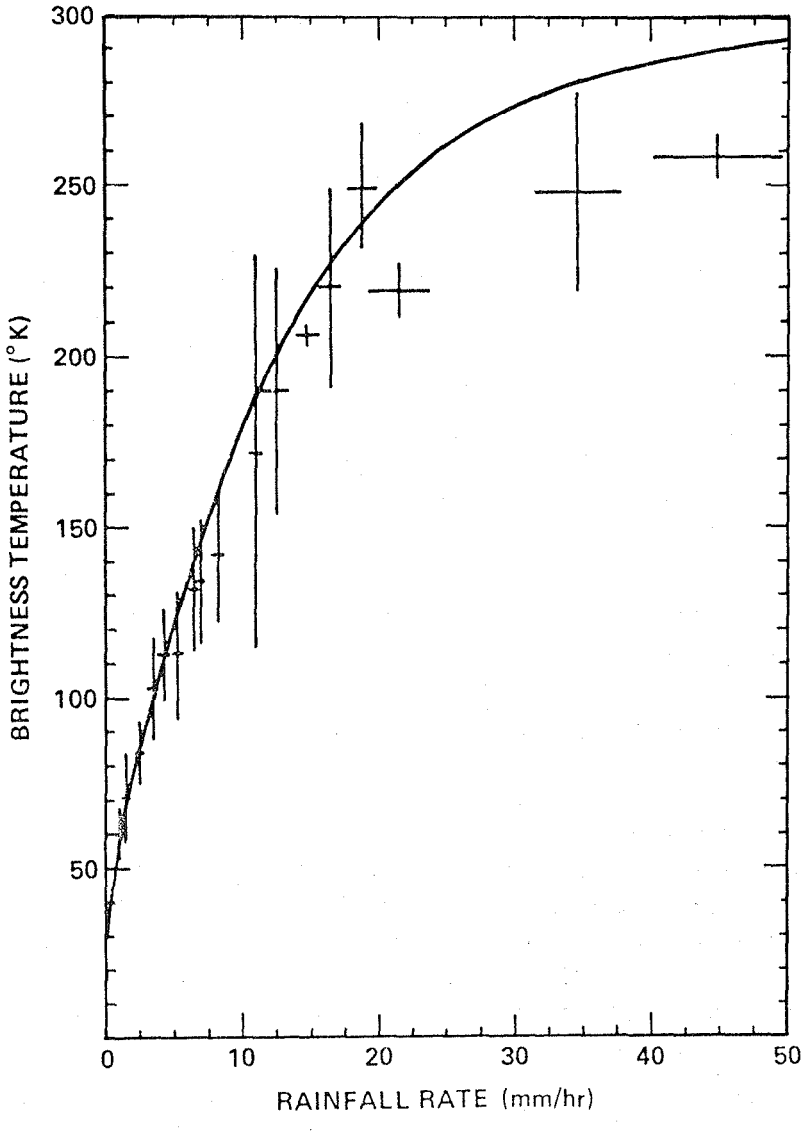

Figure 4.5: Ground-based brightness temperature observations at a frequency of 37 GHz and a view of 45 degrees from the zenith as a function of directly measured rain rate.

of about 7 km/sec. This will provide an imaged area of 3×10^{10} km^2/month. The correlation length of rain varies geographically and according to rain type, but 10 km is a typical value. Since this correlation length is less than the resolution, the number of independent samples is resolution-limited. Thus the imaged area can be considered as 10^8 samples/month.

The probability of any cell containing precipitation is similarly variable but 1% is typical, leaving about 10^6 rain samples/month globally. On a monthly basis, each 2° square of the earth would average the 100 samples required to derive a 10% estimate of integrated rainfall. Even at the lowest SSM/I frequency, this criterion would be met by approximately 5° cells. Clearly, this sort of sampling is adequate only for problems on climatological space and time scales; it is grossly inadequate for flood forecasting and other problems of short space and time scales. Of course, the diurnal cycle introduces additional complications, as yet unknown.

The large spatial component of variability causes another microwave-peculiar error source. Spatial resolution is difficult to achieve in microwave sensors due to diffraction in the antenna aperture. The SSM/I will have only about a 60 km resolution at the same frequency, 19.35 GHz. The resolution will be about 30 km at 37 GHz, but this frequency saturates at rather low rain rates in the emission mode.

Figure 4.4 shows that the transfer function between rain rate and brightness temperature is highly nonlinear; in fact, in a linear plot it is concave downward. Because of this nonlinearity, if there is any inhomogeneity in the field of view, direct application of the transfer function causes an underestimate of the rain rate. This results in a significant bias in the measurements when a great many observations are averaged. Estimates vary as to how much of a problem this was in the 25 km ESMR data; there were no extensive studies to estimate and correct for this bias. Nevertheless, the Rao, *et al.* (1976) atlas and the Adler and Rodgers (1977) tropical storm study produced quantitatively reasonable results with no correction for partial filling of the antenna beam with rain.

It can be concluded that at the 25 km resolution of ESMR, the so-called "beam filling" problem is serious but not crippling. The SMMR-SSM/I resolutions are a different matter. Studies have been made (Spencer, *et al.*, 1983), but the problem is extremely serious and requires careful study and correction.

The water vapor dependence of the brightness temperature is another degree of freedom which can introduce errors in the determination of rain intensity. The water vapor is a function of the freezing level in the model, but this only approximates reality. This error source also requires study.

It is difficult to envision high-quality precipitation estimates being derived from SSM/I data alone. A truly useful global precipitation measurement system, in addition to the existing operational capabilities, must include a polar orbiting radiometer system with frequencies similar to the SSM/I but with substantially better spatial

resolution. The SSM/I data still will be useful in order to progress toward this needed rainfall measurement system. The data may be used to develop and test algorithms for the retrieval of rainfall rates and for the combination of differing types of rainfall estimates. Moreover, even if the rainfall estimates are not so quantitative as desired, they may be interpreted as rainfall indices so that interannual variability can be examined. Over the ocean, a dearth of ground truth is the standing problem for the foreseeable future. This problem must be solved for significant progress to be made.

4.2 The GEOSAT Mission

GEOSAT will collect topographic, backscattered power (wind), and waveform data from a non-repeat orbit (near 3-day repeat, similar to SEASAT) for a period of up to 18 months. Doppler tracking via the Defense Mapping Agency's (DMA) TRANET system will provide SEASAT-quality (1 meter absolute accuracy) orbits. GEOSAT's initial and primary mission is the collection of global sea surface topographic data to be used for computing a high spatial resolution mean sea surface via groundtrack crossover point minimization in order to approximate the marine geoid. The basic approach will be to fill in the spatial gaps left in global groundtracks not covered by SEASAT. After 18 months, GEOSAT will be moved into a repeating or collinear orbit.

The primary objective of GEOSAT range data collected during the initial, or geodetic, mission is to satisfy operational needs of military inertial and strategic navigation systems. Thus, research users of these topographic data are faced with a number of logistical (raw range measurements are classified) and technical (initial orbit lays down non-repeating groundtracks) restrictions. Nevertheless, a number of oceanographic research objectives can be met within these confines, particularly during the GEOSAT-ERM mission.

4.2.1 The GEOSAT Satellite

GEOSAT consists of an improved SEASAT, single-frequency (13.5 GHz) radar altimeter mounted on an improved GEOS-C bus. Unlike SEASAT and proposed future oceanographic altimeter systems (*e.g.*, N-ROSS, TOPEX, ERS-1), GEOSAT lacks both a microwave radiometer for water vapor range correction and a laser retroreflector for range calibration. These deficiencies result in both diminished range determination accuracy (relative to TOPEX specifications) on longer spatial scales (due to orbit determination error) and some loss of precision on intermediate scales due to water vapor uncertainties. Studies (Born, 1983) indicate that absolute range accuracy of order 50 cm is feasible for GEOSAT, although a conservative error estimate is an orbit accuracy of about 1 m.

The instrumental noise is approximately ± 2 cm ($1\ \sigma$) in range in a one-data-point/sec average of the 10 points/sec raw data stream. This represents a significant enhancement over the approximate ± 3.5 cm ($1\ \sigma$) noise in similarly averaged SEASAT altimetry. This enhancement is possible given three modifications of the SEASAT altimeter design (Kilgus and MacArthur, 1984):

(a) Factor of 2 wider gate window for tracking,

(b) Diminished time lag for AGC resets,

(c) Enhanced instrument range and range rate digitization.

As well, a dual mode tracking strategy is implemented on GEOSAT by which a threshold detector on the leading edge of the return pulse is used in addition to the middle gate used in SEASAT to reset the tracking lock. This allows for an enhanced ability to maintain lock over more rugged terrain and ice than was possible with SEASAT. Total terrain excursions over which lock is maintained are the order of ± 10 m, or somewhat greater.

A key hardware modification on SEASAT design is the use of long-pulse, lower-power waveforms. This allows for the use of a long-lived, low-power, 20-watt Traveling Wave Tube Amplifier (TWTA) as opposed to the short-lived, 2000-watt SEASAT TWTA. The longer-lived TWTA and the relative simplicity of the overall GEOSAT satellite system result in probabilities of post-launch survival which exceed 50% for approximately 3 years (double the required geodetic mission duration).

4.2.2 GEOSAT Exact-Repeat Mission

Given limitations on the ultimate obtainable accuracy of GEOSAT's range measurement due to residual orbit error, it is not feasible to pose detailed, long spatial scale (order of about 10^4 km) circulation experiments, such as the global mean circulation experiment to be undertaken by TOPEX. On the other hand, on spatial scales of order 10^3 km or less (oceanic mesoscale), residual orbit error will be removed with a precision somewhat better than SEASAT, allowing collection of meaningful sea surface topography.

The critical limitation on attempts to use GEOSAT altimetry for ocean circulation studies, particularly for mesoscale oceanography, is the non-repeating nature of the altimetric groundtracks during the primary 18-month mission. Hence, in order to derive absolute topography (as opposed to topographic variability) from these data, some reference surface (composed of past altimetry and/or gravimetry) must be removed. For this purpose DMA has agreed to permit use of a classified, blended, gravimetric/altimetric surface in the Northwest Atlantic for the computation of subsequently unclassified residuals. Additionally, topographic variability can

be derived globally at crossover points even during the initial non-repeating orbit phase of the mission.

Gravimetric or mean surfaces with adequate precision and spatial resolution for mesoscale oceanographic interpretation exist in only a few regions. In a vast majority of regions, exactly repeating groundtracks which overlap to within a few kilometers or less are essential to meet many oceanographic objectives. Hence, GEOSAT's nominal mission has been extended to include a period of two years, during which time the satellite's groundtracks repeat in a nominal 17-day period (GEOSAT-ERM). This will be discussed further in Section 4.3.2. In such an orbit, crosstrack separations of 165 km equatorial (roughly 100 km at mid-latitudes) allow for minimally adequate spatial coverage with nearly adequate temporal sampling for studying the dynamics of western boundary currents. Studies indicate that stationary ensemble mean topography along each track can be obtained with precision of 10 cm or better after several months' mission duration (Mitchell, 1984), thus allowing for subsequent removal of mean sea level along each ground track.

4.2.3 Wind Speed Measurements Via the SEASAT Altimeter

The SEASAT altimeter (ALT) was an active radar which transmitted 13.5 GHz microwave radiation and measured the power of the radiation backscattered from the sea surface. For ALT measurements at satellite nadir, the normalized radar cross-section, σ°, is inversely related to wind speed. Estimation of wind speed from ALT is thus a two-step procedure. First, σ° is computed from parameters measured by the ALT receiver. Then the wind speed is computed from σ°. Accuracy in ALT wind speed estimates thus depends on either the σ° algorithm or the wind speed model function (or both). The σ° functions derived from SEASAT altimeter for retrieval of wind speed are presented in this section. For details of how σ° is obtained, see Chelton and McCabe (1985).

In the near-nadir regime (incidence angles less than 10°), σ° appears to obey a power-law relation to the wind speed. This apparently was first noted by Barrick (1974) from an analysis of aircraft nadir radar measurements made by Raytheon in 1969 and 1970. Consequently, a power-law relation is also adopted for nadir-regime SASS backscatter measurements. If σ° is expressed in dB, the power law relation becomes

$$\sigma^\circ(dB) = 10\,[G + H\,log_{10}\,u_{19.5}]$$

where $u_{19.5}$ is the wind speed at 19.5 m above the sea surface.

Reliable estimates of the constants G and H are difficult to obtain without a carefully coordinated *in situ* measurement program. Unfortunately, there was no such field program during SEASAT. A search of National Data Buoy Office (NDBO)

buoy measurements during the SEASAT mission yielded only 14 independent observations within 3 hours and 100 km of ALT σ° measurements. This small number of matches is due to infrequent buoy samples ($\sim$ every 3 hours) and the narrow "swath width" (10 km) of ALT. Clearly, 14 observations are too few to derive an ALT wind speed model function.

Chelton and McCabe (1985) propose an alternative method of model function development. They compare spatially and temporally averaged ALT measurements of σ° with similarly averaged vertical polarization, off-nadir scatterometer measurements of wind speed. Scatterometer wind speed measurements are generally believed to be as good as or better than all but the highest quality *in situ* measurements. Because of the different sampling characteristics of the two instruments, the averaging time must be long and/or the spatial averaging must be large for a sensible comparison between ALT and SASS measurements of a spatially and temporally varying wind field. After experimenting with spatial averaging sizes, 2° latitude by 6° longitude was chosen; smaller averaging increased the scatter in the data, presumably due to under-sampling by ALT. To maximize the reliability of the model function, a 96-day average over each 2° by 6° region (the full length of the SEASAT mission) was used.

A scatter plot of global 96-day, non-overlapping 2° by 6° average ALT σ° and SASS $u_{19.5}$ is shown in Figure 4.6. The solid line in the figure corresponds to the proposed new model function. The G and H values (1.502 and -0.468, respectively) derived for the global data set are an adequate representation in all geographical regions. Inverting the proposed algorithms to obtain the 19.5 m wind speed from measurements of σ° gives

$$u_{19.5} = 10^{[(\sigma(dB)/10 - G)/H]}.$$

A scatter plot comparison of 96-day, 2° by 6° average SASS wind speed is shown in Figure 4.7. The correlation between the two estimates of wind speed is 0.94 over a range from 4 to 15 m/s. The slope of the least square fit straight line is 1.005 ± 0.048 with an offset of (0.084 ± 0.409) m/s and an rms error of 0.82 m/s. It should be borne in mind that the validity of the proposed algorithm has been demonstrated only on spatially and temporally averaged data. Work in progress at Oregon State University and Remote Sensing Systems is extending the range of the ALT wind speed model function beyond the 4–15 m/s range available from 96-day 2° $\times$ 6° averages.

A natural question that arises is whether the proposed algorithm adequately describes instantaneous ALT estimates of wind speed. A rigorous test of performance on individual measurements of σ° requires an extensive high-quality *in situ* data base for comparison. Since only 14 independent buoy observations were available during SEASAT, a meaningful comparison with instantaneous wind measurements is not possible. However, Chelton and McCabe (1985) show that the accuracy of

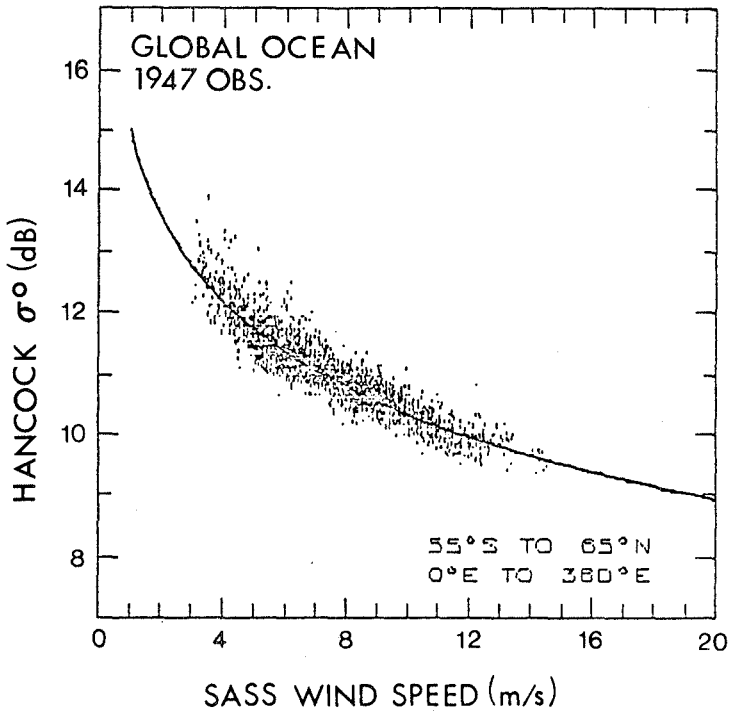

Figure 4.6: Scatter plot of global 96-day, non-overlapping 2° by 6° average σ° (computed using the Hancock modified algorithm) as a function of SASS wind speed (corrected for a 1 m/s bias). Continuous curve shows least square fit to the data.

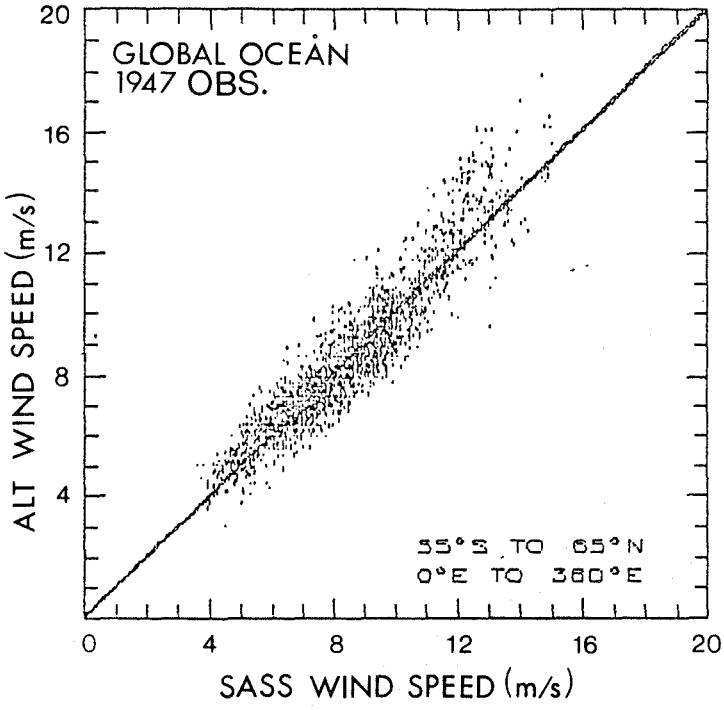

Figure 4.7: Scatter plot comparison of 96-day non-overlapping 2° by 6° average SASS and ALT wind speeds (corrected for a 1 m/s bias). Straight line represents perfect fit.

SEASAT σ° measurements was ± 0.3 dB. This error translates to a 0.5 m/s error when the true wind speed is 8 m/s and a 4 m/s error when the true wind speed is 20 m/s.

It would seem that ALT wind speed estimates will be most useful when the data are temporally and spatially averaged. Thus far, only 96-day 2° × 6° averages have been examined. The lower limits of averaging are the subject of further investigation. This problem, unfortunately, is addressable to only a limited degree from SEASAT data because of intermittent sampling by ALT during the 96-day mission.

4.3 SSM/I and GEOSAT Coverage

Two kinds of information are required to characterize the coverage of a satellite remote sensing system. First are the instrument and orbit characteristics defined by the system's engineering and test data. Secondly, adequate preliminary understanding of the phenomena to be studied and the level of description in the desired results are needed. An observing system may be suitable for a study of annual mean

basin-scale circulation, but quite useless for describing the barotropic effects in the wake of a rapidly moving storm.

To keep this discussion within manageable bounds, the most important of the observing system parameters for SSM/I will be enumerated and a few illustrative cases will be presented. GEOSAT will be similarly considered. However, it must be determined by the individual investigator whether these observing systems can serve the purpose.

There are three scales of sampling characteristics. The smallest refers to the individual primitive observation and is associated with spot size, field of view, cell size, dwell time, and integration time, or similar terms. The second scale group is made up of sample spacing (both along- and across-track), overall swath width, interswath gap width, and revisit time. Finally, the largest scales are the dimensions of the sample domain and the length of record. Here swath and domain scales will be emphasized, rather than field-of-view scale parameters.

4.3.1 SSM/I Coverage

The swath of SSM/I is generated as illustrated in Figure 4.1. Fields of view and integration times are given in Table 4.2 for the individual channels. With the orbital characteristics in Table 4.3, a pattern resembling that in Figure 4.8 is painted out by the ground track. The inter-orbit gap, S, is 25.4°. Counting both ascending and descending passes, the coverage consists of a diamond-shaped mesh, as shown in Figure 4.9.

This coverage would be adequate for ocean surface wind speed, sea surface temperature, and integrated water vapor in many oceanographic and air-sea interaction studies, including basin scale models, for which 100–200 km resolution and a sampling interval, or averaging time of a few days, usually are desired.

Near the equator, the characteristic size of the mesh is about half of 25.4°, or 1394 km. The acute angles of intersection, or the "points" of the diamonds, are about 40° near the equator. The exact patterns, including the symmetry properties of the uncovered areas, are functions of the numbers of days and orbits in a repeat cycle. The approximate numbers of intersections per day are shown in Table 4.4. On the average, the intersections are about 780 km apart, but it is clear from the table that they become much closer together as latitude increases, until they are 220 km apart for the most poleward intersections. This pattern migrates westward and nearly repeats at six-day intervals. For most purposes, even this is longer than the effective revisit time, since the 1394 km swath width very nearly gives daily coverage of the equator, double coverage (*i.e.*, twice daily) for half of the subtropics, and double coverage poleward of about ±60° latitude (Figure 4.10).

Oceanic rain is important to the salt budget of the surface layer. Over land, total rainfall is highly variable, and, in some regions, a seasonal total is made up

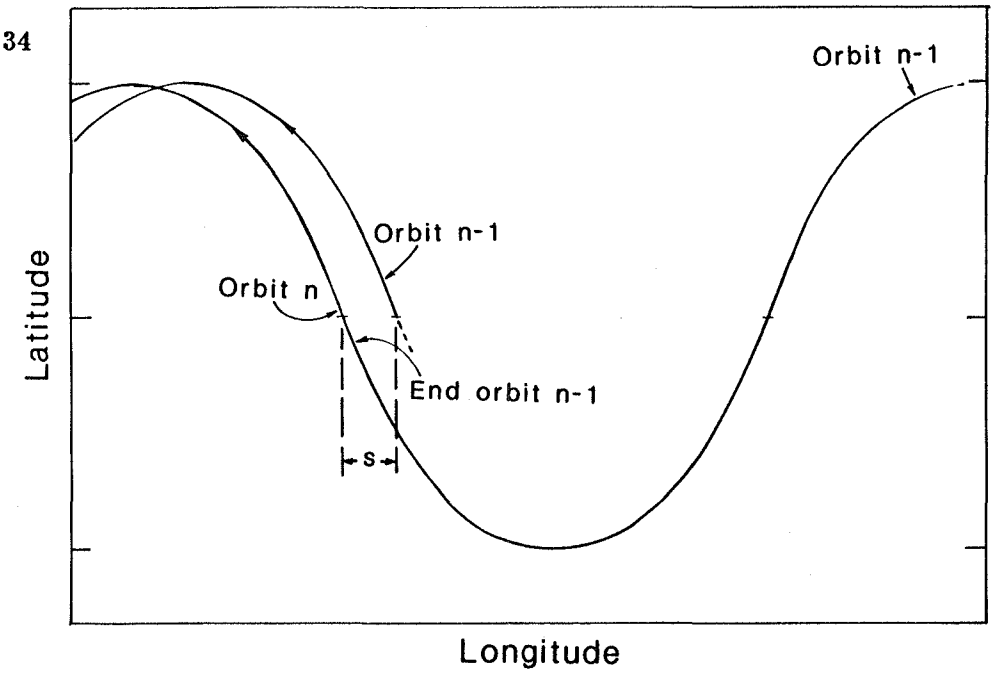

Figure 4.8: Relationship of successive ascending nodes for retrograde orbits (inclination greater than 90°). For DMSP SSM/I, the values of S is 25.4°; for Extended GEOSAT, S is 24.8°.

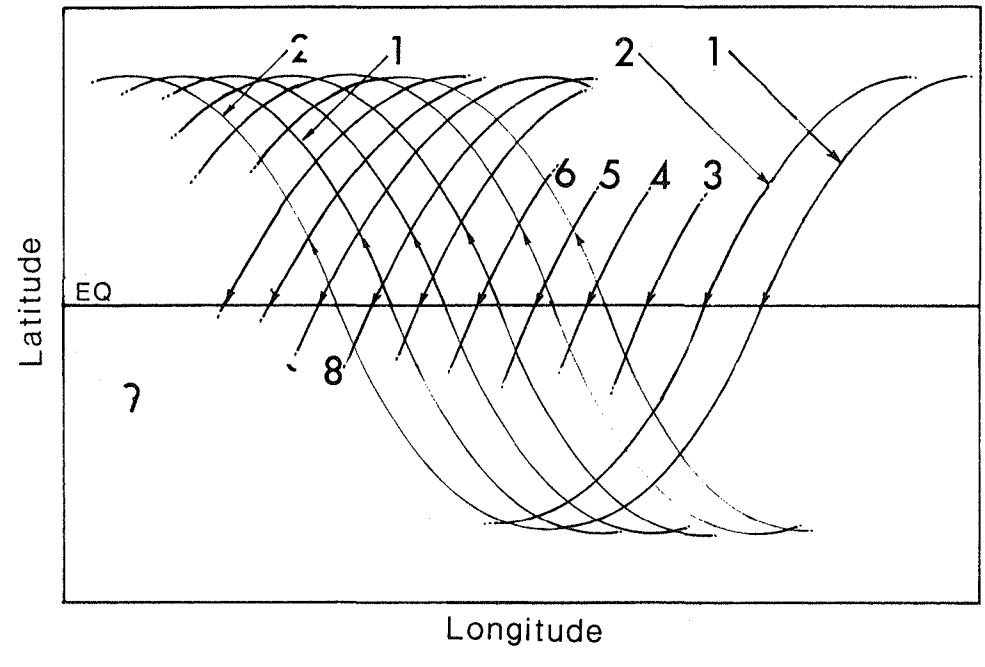

Figure 4.9: Pattern of subsatellite tracks built up in one day. Numbers are relative orbit numbers. Since one day is less than the repeat time, the descending nodes neither coincide with the ascending node nor evenly divide them. Thus, the pattern is neither symmetrical nor anti-symmetrical. For SSM/I the ratio of the short equatorial segments to the long segments is about 2/3; for GEOSAT the ratio is about 1/4.

Table 4.2: SSM/I Characteristics.

Center frequency (GHz)	19.35	22.24	37.00	85.50
Polarization	V,H	V	V,H	V,H
Brightness resolution (°C)	0.8	0.8	0.6	1.1
Field of view (axes of approximate ellipses at 3 dB points, km)	70×45	60×40	38×30	16×14
Swath width (km)	1394	1394	1394	1394
Integration time (m/s)	7.95	7.95	7.95	3.89

Table 4.3: Approximate Orbital Characteristics for DMSP SSM/I.

Orbit type	circular, sun-synchronous
Orbital period (sec)	6085.3
Altitude (km)	833
Inclination (deg)	98.7
Approximate repeat cycle (days; orbits)	6(85)

Table 4.4: Distribution in Latitude of Orbital Intersections for Several Inclination Angles in 15 Orbits (somewhat greater than 1 day for DMSP and GEOSAT).

Latitude Range (deg)	Inclination Angles (deg)			
0–5	0	0	0	0
5–10	0	0	0	0
10–15	0	0	8	8
15–20	0	8	0	0
20–25	8	0	8	8
25–30	0	0	0	0
30–35	8	8	0	0
35–40	0	0	7	7
40–45	0	0	9	9
45–50	0	0	0	0
50–55	0	0	6	6
55–60	7	7	10	10
60–65	9	9	5	16
65–70	0	6	27	19
70–75	16	10	33	30
75–80	32	35		
80–85	33	30		
Total per hemisphere	113	113	113	113

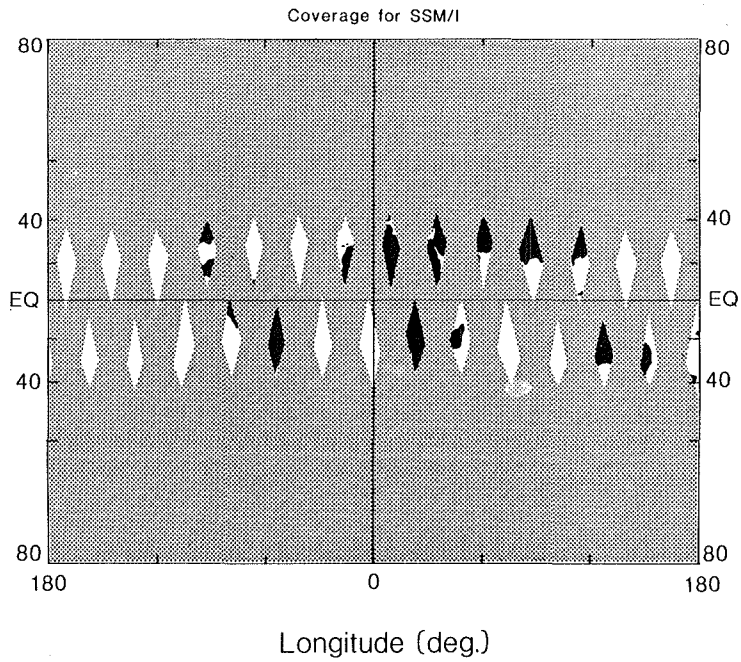

Figure 4.10: Schematic coverage for one day of SSM/I data.

of a small number of "events." As presented in Section 2.4, a similar phenomenon occurs in some ocean regions. There SSM/I time sampling may be inadequate to obtain rainfall at scales of the order of the footprint (Figure 4.11). In order to fill this area completely with observations, five days of Nimbus 7 SMMR data had to be composited. It may be necessary to average over larger areas to obtain valid rain estimates. Even on a monthly time scale, rain events recovered from the Nimbus 7 SMMR data are "granular" rather than smooth, as shown in Figure 4.12. There is ambiguity between rain rate and rain area arising from the failure of some rain cells to fill an entire field of view. However, this may be less a problem with the 13 km field of view of the 85.5 GHz channels on SSM/I than the lower frequency data from SEASAT and Nimbus spacecraft.

SSM/I wind information will be regarded as incomplete by those requiring wind direction. Some advantages may be expected from SSM/I data even if direction has to come from another source, since competing data sources may have less skill in speed determination.

4.3.2 GEOSAT Coverage

The primary geodetic mission goal of GEOSAT is to provide global sea surface topography with a cross-track spacing of approximately 5 km. To achieve this, a

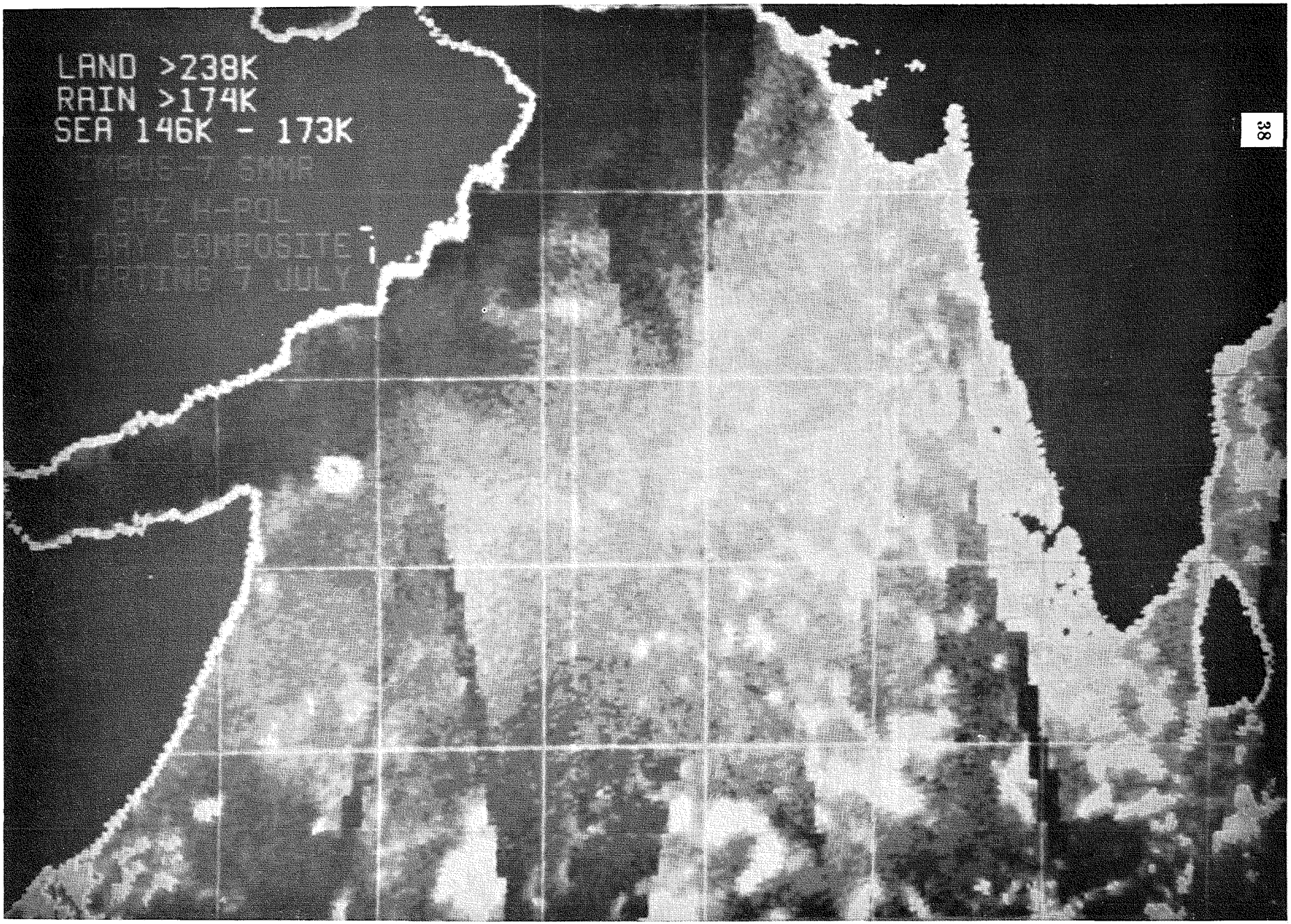

Figure 4.11: Rain events in a five-day composite image from the SSMR GHz channel H-polarization (Spencer, 1984, private communication).

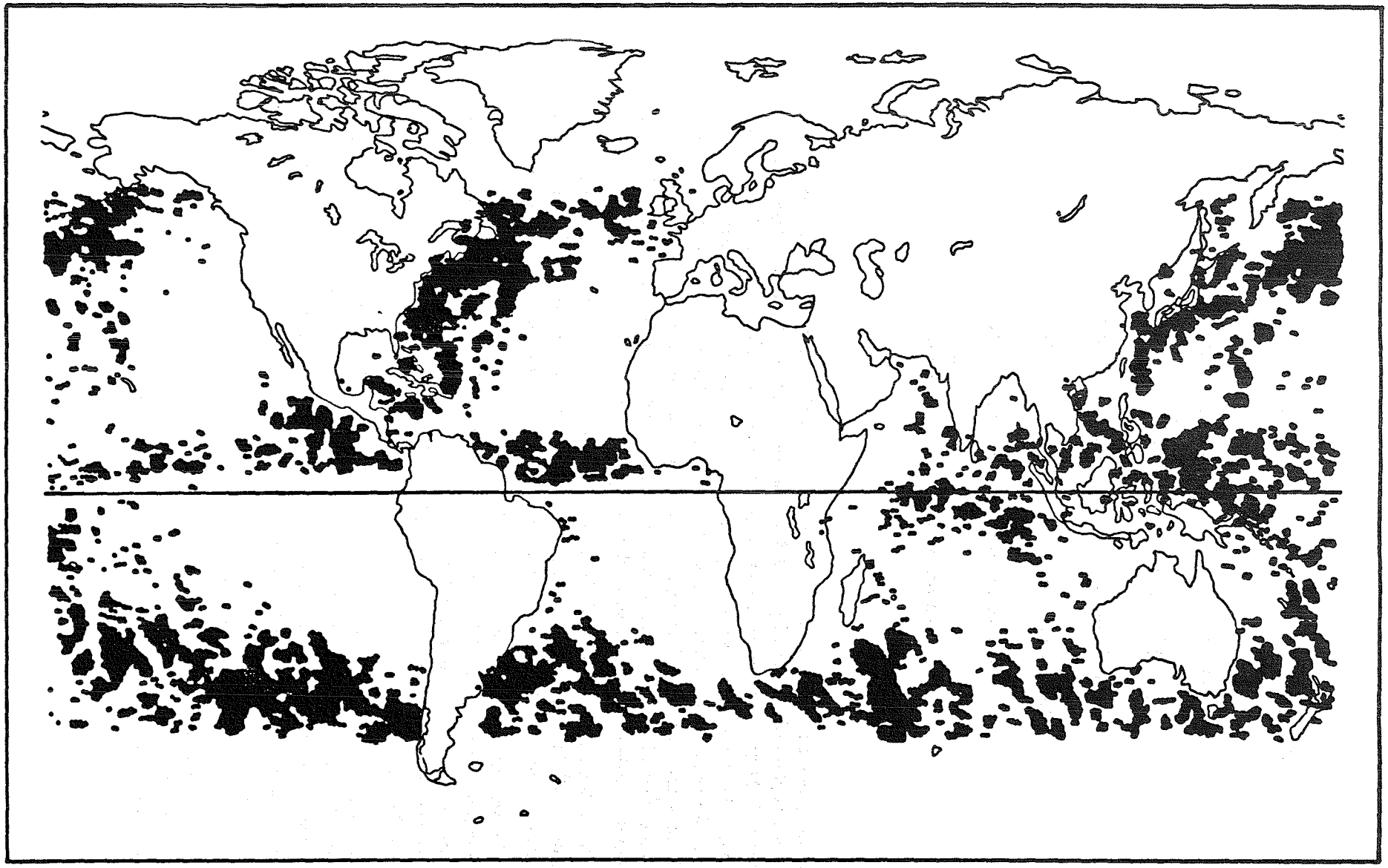

Figure 4.12: Convective rain events from Nimbus 7 SMMR data according to an experimental algorithm developed by Spencer (1985). The data are from a 17–day period distributed throughout June 1980. About 19,000 events are recorded. No correction has been applied for the increased sampling per unit area at higher latitudes.

Table 4.5: Nominal Orbital Characteristics for GEOSAT

Orbit Type	Geodetic Mission	ERM
Orbital Period (sec)	6040	6037.48
Altitude (km)	800	800
Inclination (deg)	108	108
Repeat Cycle (days)	non-repeat*	17

* Lowest-order near-repeat is 3 days.

nominally non-repeating orbit with inclination of 108° and period of approximately 6040 sec is planned (Table 4.5). A D-day repeating orbit will have an integer number of orbits in D-days. However, even though it is possible to choose an orbit that never repeats, the ground track eventually will come close to some near-repeat. The orbit chosen for the initial geodetic GEOSAT mission has a lowest-order near-repeat cycle of 3 days and is expected to repeat within approximately 5 km in 18 months. A regional view of 30 days of accumulated ground tracks is shown in Figure 4.13, and the global scale coverage for three days is shown in Figure 4.14.

As in the case of SSM/I, daily coverage is characterized by a cross-track spacing of $\sim 10^3$ km. The spatial and temporal separation of the revisited sites will determine the space-time scales that are observable, as discussed earlier for SSM/I.

To facilitate oceanography, the GEOSAT-ERM will begin with a change in orbit during fall, 1986. The GEOSAT-ERM orbit has been designed specifically to allow observation of changes in ocean topography due to mesoscale variability with time scales below 10^2 days and space scales of $\sim 10^2$ km. The non-stationary nature of this eddy field is a major consideration.

In order to avoid aliasing, one must have enough satellite passes to define mesoscale eddies spatially in the time they move a distance comparable to their size; otherwise, they lose their identity. Based on simulation studies, an orbit with a repeat time of 17 days has been selected for the GEOSAT-ERM. Figure 4.15 illustrates the regional coverage that such an orbit would accumulate in 17 days. This orbit has a nodal period of about 6038 sec, equivalent to 14–6/17 orbits per day.

The sequential ascending sub-satellite tracks or sequential descending sub-satellite tracks will be spaced about 25.8°, or 2733 km, apart near the equator (see Figure 4.9). Because of the interleaving of ascending and descending passes, the

equivalent mesh dimension averages about 12.4°, or 1364 km. The approximate distribution of latitudes of the mesh intersections for one day is found in Table 4.4.

In terms of wind and wave observations, the coverage is quite anisotropic. As the very thin radar pulse (less than one meter thick) from the altimeter impinges on the sea surface, the disk-shaped area of contact first grows in area, becomes annular, then falls to zero after the outer edge of the antenna beam has been reflected. As mentioned in Section 4.2.3, the strength of the radar return depends upon the slope distribution, or roughness, which is primarily determined by wind speed. Since the pulse is very thin and nearly tangent to the sea surface as reflection takes place, the elevated areas penetrate the pulse volume and become illuminated, while depressed areas remain unilluminated. The net effect is that wave height affects the pulse shape.

The relevance of this overly simple description is that although equivalent spot size and swath width vary with wave height, they are usually of the order of 10 km. Relative to the inter-orbit separation, the along-track sampling is essentially continuous and the swath very narrow. Therefore, a map of the sub-satellite point is nearly equivalent to a spatial picture of the sampling function, W (Figures 4.9, 4.13, 4.14, and 4.15).

From the standpoint of wind and wave observation, even daily observations having a longitudinal resolution of 12.4° would be extremely useful as a supplement to other observations in monitoring basic scale wind and stress fields. Moreover, in the southern ocean, where there is very little *in situ* data, even daily data with 12.4° longitudinal resolution are valuable because of their regular distribution.

Like SSM/I, a serious impediment to the use of GEOSAT wind observations appears to be the lack of accompanying directional data, which must therefore be obtained from another source, such as ships, surface pressure analyses, or cloud motions.

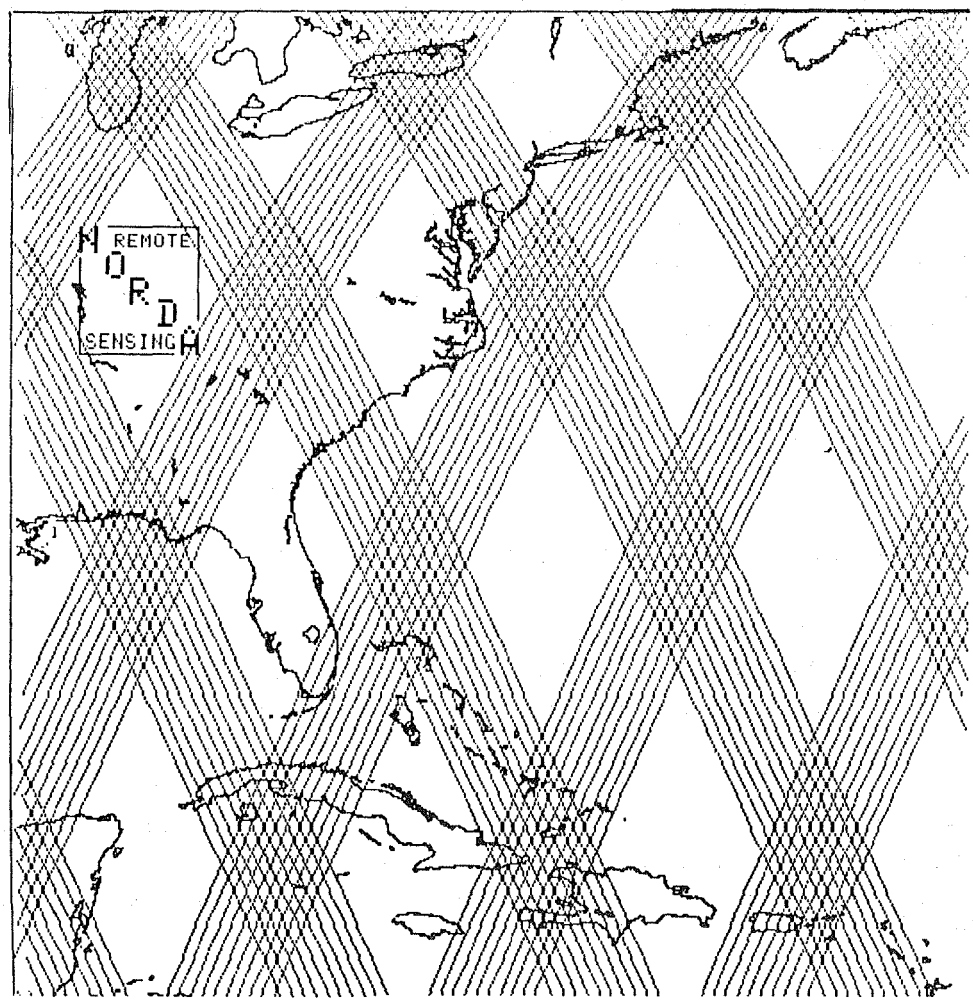

Figure 4.13: Regional ground track coverage for 30 days during the initial GEOSAT Geodetic Mission.

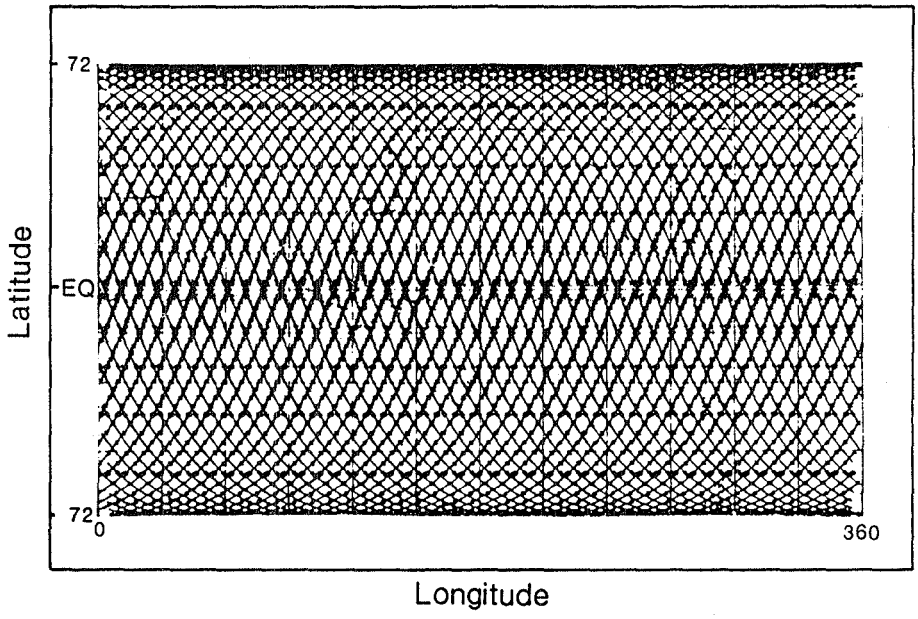

Figure 4.14: Three-day global-scale ground track coverage during the initial GEOSAT Geodetic Mission.

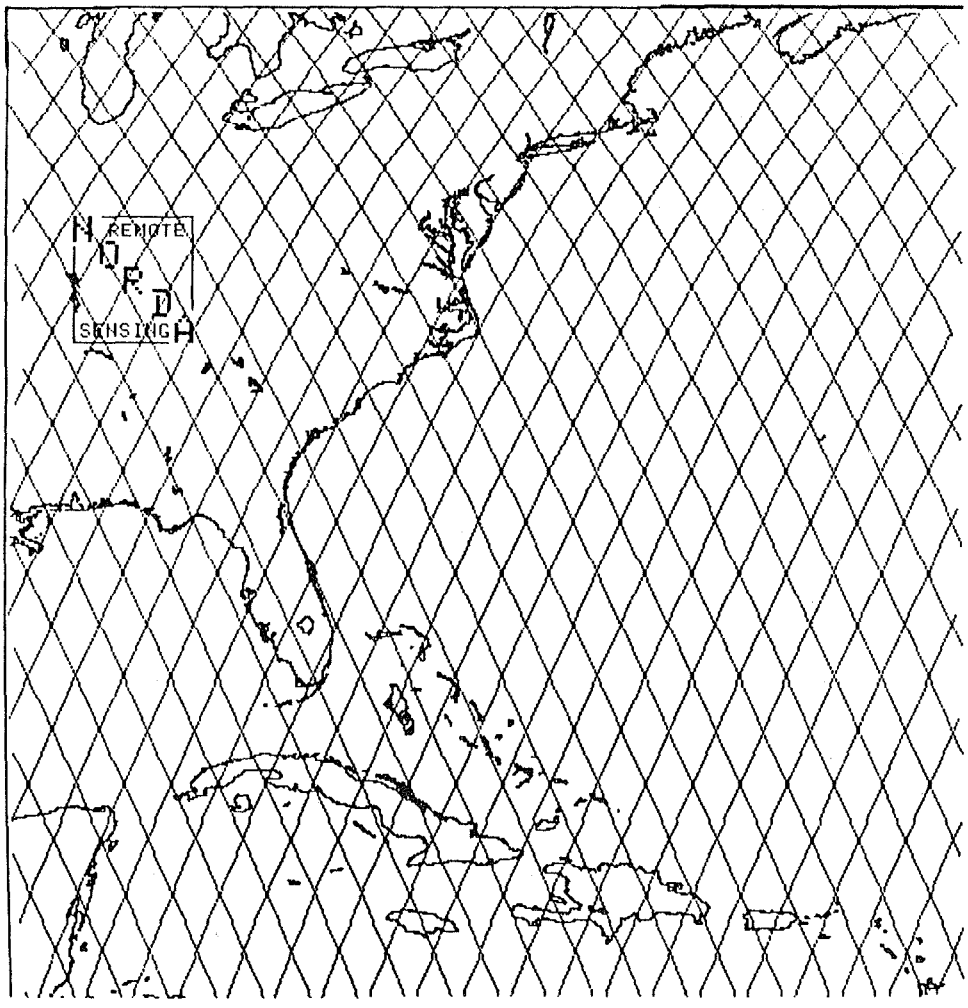

Figure 4.15: Twenty-day regional coverage for an exact repeat orbit during Extended GEOSAT.

5 SSM/I DATA SETS

5.1 SSM/I Antenna Temperature Data Set

Conversion from Level I (engineering units) to Level 1.5 (antenna temperatures) involves a radiometric calibration. The algorithm for performing this calibration has been developed by Hughes Aircraft Company (1980). Output raw data from the radiometers is given in volts (or equivalent "counts"), which are converted to antenna temperatures (Kelvins) via a calibration algorithm. The algorithm compensates for losses in the radiometer and antenna system, and for variations in ambient temperature of the instrument. The equation has the form:

$$T_{Ai} = A + BV_i \tag{3}$$

where V_i is the raw data voltage for the i^{th} channel, and A and B are functions of radiometer ambient temperature, T_R. The functional forms of A and B, and the coefficients therein, are derived from a physical model of the radiometer system with empirical adjustments based on data from thermal vacuum calibration tests. Documentation of these calibration tests and the calibration coefficients should be made publicly available so that long-term monitoring of the instrument calibration can be performed after launch.

It is the intention of the Fleet Numerical Oceanography Center (FNOC) to provide sufficient calibration data along with the T_A's so that the raw data (*i.e.*, radiometer counts) will be recoverable from the T_A's. Thus the T_A data set represents the fundamental sensor data set. FNOC will be sending the T_A's to NESDIS for archiving. FNOC also may send brightness temperatures (T_B) to NESDIS, depending on the availability of computer resources. The T_B's represent a weighted average of T_A's, and as such it will be difficult, if not impossible, to recover the T_A's from the T_B's.

The purpose of computing T_B is to correct for the antenna pattern effect, which is folded into the T_A. However, there is some debate as to the best way to account for antenna pattern effects. There is also uncertainty in the antenna pattern coefficients required to convert the T_A's to T_B's. If the baseline antenna pattern coefficients are in error, then the T_B's will have to be recomputed. For these reasons it is likely that some users will prefer the T_A's to the T_B's. Therefore, it is desirable to archive the T_A's instead of the T_B's. The computer storage requirements are the same, since there is a one-to-one correspondence between T_A and T_B. Further, T_A to T_B conversion algorithms such as FNOC's are fairly simple and easily implemented.

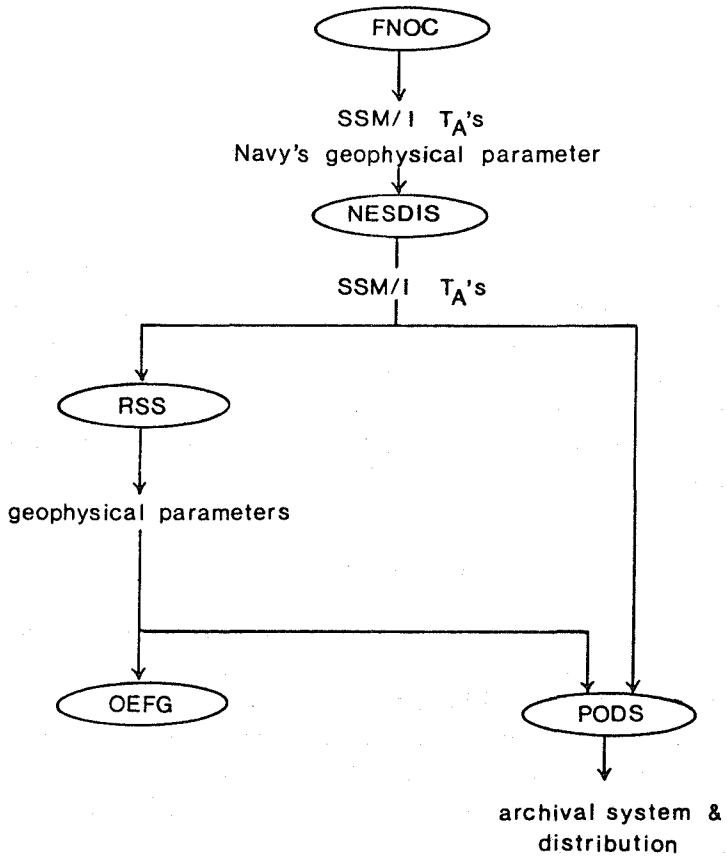

Figure 5.1: Data flow for NASA's geophysical processing of SSM/I data.

5.2 SSM/I Geophysical Data Set

NASA plans to produce and archive an SSM/I geophysical data set that will be tailored to the needs of the oceanographic and meteorological communities. To accomplish this, algorithms will be developed to convert the SSM/I T_A's (or T_B's) to wind speed, water vapor, and rain rates. One such geophysical algorithm is being developed by Remote Sensing Systems (RSS). RSS is planning to receive weekly a magnetic tape from NESDIS containing the SSM/I antenna temperatures. These T_A tapes will be converted to geophysical data tapes, which will then be sent to the Pilot Ocean Data System (PODS).

Two types of geophysical data will be produced: high-resolution and low-resolution. The high-resolution parameters will be located along the SSM/I scan lines, while the low-resolution parameters will be averaged into latitude and longitude bins for a specified time period. Figure 5.1 illustrates the data flow involved in this geophysical processing. PODS also will be receiving the T_A's from NESDIS in support of the Sea-Ice Algorithm Working Group. There are no plans currently for using the operational geophysical products that will be produced at Fleet Numerical Oceanography Center (FNOC).

5.3 PODS SSM/I Archival Plans

The following discussion summarizes the current archival plans of the Pilot Ocean Data System (PODS) for the SSM/I data sets. Although most of the discussion is directly pertinent to the Ocean Surface Energy Fluxes Working Group, the higher level data sets described have been specifically requested by the ice science community. As a result of information obtained at the Sea-Ice Algorithm Working Group (SAWG) meeting held at NASA/ Goddard on April 25–27, 1984, the details of the PODS SSM/I archival plans are less certain than previously thought. Additional discussion of the PODS SSM/I archival plan can be found in Bonbright (1984).

5.3.1 SSM/I Data Flow

The data ultimately received by PODS will be processed by the Fleet Numerical Oceanography Center (FNOC) on a real-time basis for operational use by the Navy. It is expected that FNOC will produce a set of Sensor Data Records (SDR's) and Environmental Data Records (EDR's). The SDR's consist of Earth-located brightness temperatures that have been surface type-tagged, calibrated, and antenna-corrected. The EDR's are geophysical parameters computed from the SDR's. The Navy also will provide antenna temperatures (T_A's), the data from which the brightness temperatures are calculated.

Currently, PODS is planning to receive the SSM/I data from NESDIS via magnetic tape on a regular basis. At a minimum, the data received will include SDR's, or T_A's if the the SDR's are not available. There are no current plans to archive T_A's. Whether or not the EDR's will be obtained and archived will depend on user interest.

5.3.2 SSM/I Data Processing and Archival System

The PODS SSM/I archival system is illustrated in Figure 5.2. This depiction assumes that PODS will receive SDR's and EDR's. If T_A's are received rather than SDR's, it will be necessary to add another step to create the SDR's.

Once the SDR and EDR tapes are received from NESDIS, they will be copied onto optical disk platters with only minor format changes. The EDR Tape Copy Archive will be the end product for the EDR data. These data will be available to users, but not as an on-line computer product. In contrast, the Input SDR Archive will be reorganized into a file structure that permits rapid, selective access to subsets of the data. As illustrated in Figure 5.2, it is this global coverage SDR "Rapid Access Archive" which will be used to create the higher level products.

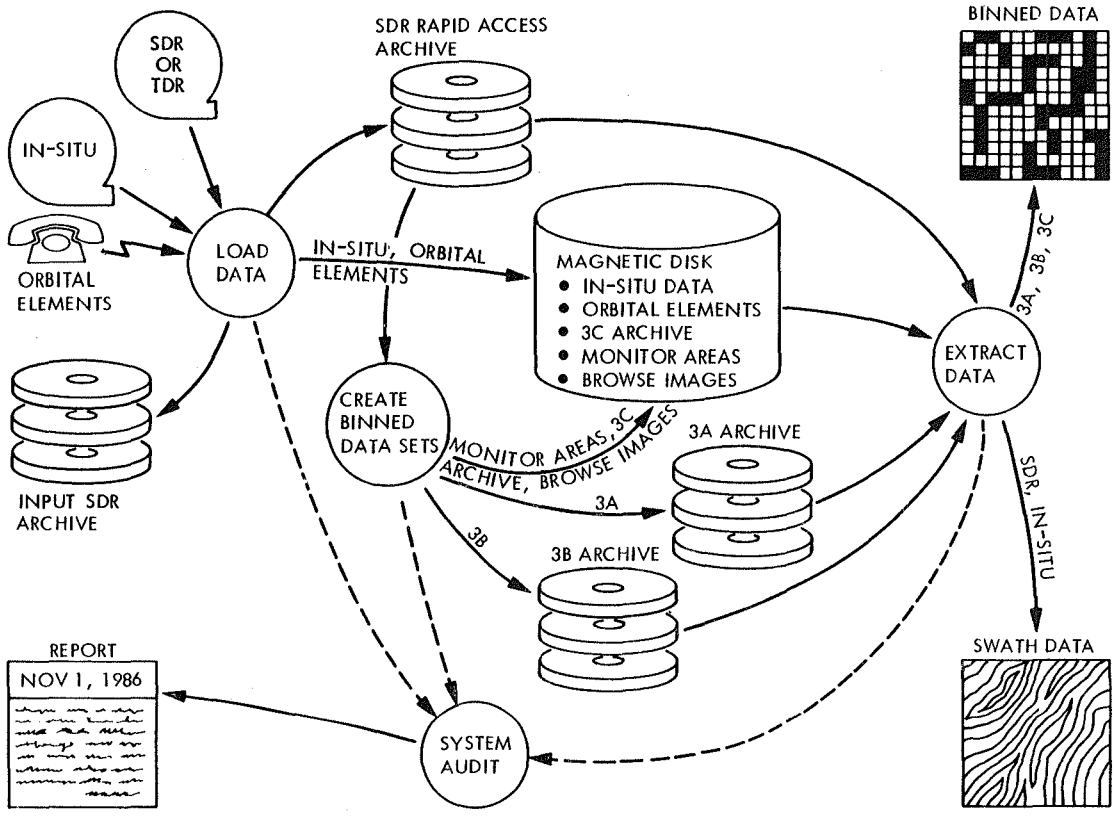

Figure 5.2: PODS SSM/I archiving system. This figure assumes that PODS will receive either SDR or TDR tapes from NESDIS.

Table 5.1: PODS: Data Level Definitions.

Level	Definition
0.0	Raw telemetry bit stream
1.0	Frame-synchronized, decommutated, Earth-located, converted to engineering units (*e.g.*, volts, amps, degrees)
1.5	Converted to sensor variables (backscatter coefficient, brightness temperature, radiance)
2.0	Converted to geophysical variables (winds, sea surface temperatures, chlorophyll)
2.5	Most supporting data deleted
3.0	Earth-fixed grid (time $\rightarrow$ geographic order)
4.0	Temporal/spatial summaries

5.3.3 Current SSM/I Level 3 Products

As defined by the processing level definitions (see Table 5.1), the T_A's are essentially Level 1.5 data, the SDR's are Level 1.5 data, and the EDR's are Level 2 data. All are swath-oriented. The Level 3 products to be created by PODS will be temporally and spatially averaged. These data will be displayed on regular Earth-fixed grids. The Level 3 archives described below cover the polar regions. All will be available on-line. Currently, the following Level 3 archives are anticipated:

(a) 3A Archive: 12.5 km brightness temperatures calculated for the 85.5 GHz channels averaged over one day;

(b) 3B Archive: 25 km brightness temperatures calculated for all channels, except the two 85.5 GHz channels averaged over one day.

5.3.4 Algorithm Development Support

PODS plans to support the algorithm development activities of the SAWG. This support will include:

(a) Implementing an interim algorithm,

(b) Maintaining validation data bases,

(c) Providing validation tools,

(d) Supporting validation workshop activities.

5.3.5 User Support

User support supplied by PODS includes:

(a) Data extraction capability,

(b) Data product generation,

(c) On-line bibliography,

(d) On-line data catalog,

(e) On-line browse files.

Products can be obtained at the terminal, on hard copy, or on magnetic tape. Graphical products include, but are not limited to, time series, contour maps, and histograms.

6 DATA PROCESSING AND VALIDATION OF DATA SETS

6.1 Geophysical Data Validation

Validation of satellite data sets will be necessary shortly after launch to develop confidence in the processing algorithms, and also during an extended post-launch period to compensate for calibration drifts and other anomalies that may have escaped earlier investigation. If several candidate algorithms exist up to the launch date, subsequent evaluation will be required to understand the significance of differences between the algorithms and to converge on a single algorithm for long-term processing.

Independently obtained measurements are necessary to validate each geophysical quantity. Accurate point measurements, such as radiosondes and buoys, can be co-located and compared with satellite data on a per-orbit basis. In other cases, measurements can be aggregated in space and time for comparison as interpolated or averaged fields. Acquisition of high-quality *in situ* data will be needed for each parameter to be validated. These data must be acquired from a sufficiently diverse range of geophysical environments, representing seasonal change as well as geographic variability.

For longer-term performance monitoring, it will be desirable to have *in situ* sensors located at dedicated calibration sites in key ocean areas that will continuously monitor ocean conditions over a period of decades. These sensors will serve to "tie down" the satellite-derived fields and identify calibration drifts in the instruments. They also will improve continuity between calibrations of similar sensors on successive satellites.

A number of experiments planned for the latter part of the 1980's will provide candidate *in situ* data for the validations stated above. These experiments include FASINEX (October 1985 – March 1986), Ocean Storms (September–November 1987), and Tropic Heat/EPOCS (October 1983 – October 1987). These experiments, in conjunction with ship-of-opportunity reports, will provide data for validating the satellite wind measurements.

Humidity data for validating the SSM/I water vapor measurements can be obtained from the network of reporting radiosonde stations and research ships, and ships-of-opportunity using ASAP (Automated Shipborne Aerological Programme) equipment distributed in the tropical and northern Pacific and Atlantic Oceans. Extensive GEOSAT altimeter topographic validation will result from the Gulf Stream Regional Study (see Section 2.5.1).

6.2 Sensor Data Validation

Anomalies in the geophysical data, which possibly may be due to geophysical algorithm shortcomings, also may be caused by anomalies appearing in the sensor level data. Thus, it will be necessary for both SSM/I and GEOSAT to have some means of monitoring the T_A's and the σ°'s, respectively, for drifts or sudden shifts in calibration, excessive noise, or other signs of sensor degradation and malfunction. Problems with sensor data algorithms also must be detected.

For these purposes calibration sites, at which the sensor data (antenna temperature or backscattering coefficient) have known or constant values, also are necessary. Therefore, plans should be made to monitor constantly a subset of the Level 1.5 data in these regions over the life of the satellite mission. Access to lower level data also must be maintained in case reprocessing is necessary to compensate at the sensor data level for anomalous sensor or calibration algorithm behavior.

6.3 Validation Workshops

For the purpose of validation at both sensor and geophysical data levels, the preferred mechanism is to hold one or more workshops to compare data sets and algorithms against each other in an objective and unbiased manner. This will require special processing of selected data sets to provide common data formats and to generate the necessary plots and statistics for evaluation. These workshops (or working group meetings) should begin prior to launch to evaluate candidate algorithms using simulated data sets and models. They should continue after launch with a frequency related to the level of maturity of the algorithms and data sets. Therefore, it is necessary that a team of user scientists and cognizant algorithm developers be kept together as a working group significantly beyond launch.

7 CONCLUSIONS

7.1 Oceanographic Parameters

The following useful oceanographic parameters can be obtained from SSM/I and GEOSAT/GEOSAT-ERM data:

(a) TOTAL WATER VAPOR, SSM/I: Synoptic + global monthly means

(b) WIND SPEED

(i) SSM/I: Synoptic + global monthly means

(ii) GEOSAT: Coarse sampling, synoptic
- Non-repeating orbit (4.5° long., monthly averages)
- Repeating orbit (2.2° long., monthly averages)

(c) RAIN RATE (liquid water), SSM/I: Synoptic

(d) SEA LEVEL: Study of time-dependent ocean phenomena

(e) $H_{1/3}$ (effective wave height): Statistics

Accuracies of all parameters depend upon averaging, retrieval technique, and climatological regime. Not all aspects have been worked out in the required detail.

7.2 Scientific Problems

The scientific problems that can be addressed using these parameters are the following:

(a) TOTAL WATER VAPOR: Analysis of synoptic storms; computation of latent heat flux and climate variability; studies of atmospheric numerical model verification.

(b) WIND SPEED: Verification of surface expressions of cloud wind speed; computation of latent heat flux; analysis of mesoscale ocean storms.

(c) RAIN RATE: Possible estimates of ocean salt budget; synoptic storms and air-sea interaction modification due to rain; a continuing, important research problem.

(d) SEA LEVEL: Topographic studies of eddies, rings, and major fronts; seasonal tropical sea level changes and planetary wave propagation.

(e) $H_{1/3}$: Statistical studies of ocean waves; wave generation models; swell propagation.

7.3 Algorithm Development

Algorithm development is required for the following geophysical parameters:

(a) TOTAL WATER VAPOR: Well developed conceptually; limited by standards of comparison; systematic biases in total water vapor.

(b) WIND SPEED: SEASAT Altimeter, wind algorithm problems; SSM/I winds very promising but not looked at so intensively as altimeter winds.

(c) RAIN RATE: Rain cells smaller than footprint, poorly resolved; important research area.

(d) SEA LEVEL: Orbit error of order 1 m (at very long wavelengths), an improvement over SEASAT. GEOSAT altimeter most useful for intermediate and shorter spatial scales; problems in computation of satellite orbits.

(e) $H_{1/3}$: Available.

8 RECOMMENDATIONS

- That the SSM/I antenna temperatures be archived.
- That the altimeter waveform be archived.
- That geophysical algorithms be developed and documented and be made available for computation by user group: wind speed, $H_{1/3}$, total column humidity, rain rate, sea level changes.
- That gridding and averaging schemes be available and documented for each geophysical parameter.
- That sensor statistics be validated early in the flight.
- That *in situ* experiments (FASINEX, Ocean Storms, Tropic Heat/EPOCS) be coordinated with SSM/I and GEOSAT investigations.
- That PODS be utilized to both store and distribute SSM/I data to research users.
- That NOAA/GDS be utilized to both store and distribute GEOSAT data. Complete documentation of the orbital and geoid errors should be provided.
- That algorithm verification and maintenance teams be established.
- That the Science Working Group be continued to ensure implementation of recommendations.

REFERENCES

Adler, R.F., and E.B. Rodgers, 1977. Satellite observed latent heat release in a tropical cyclone. *Mon. Wea. Rev.*, 105, 956-963.

Alishouse, J.C., 1983. Total precipitable water and rainfall determinations from the Seasat Scanning Multichannel Microwave Radiometer (SMMR). *J. Geophys. Res.*, 88, 1929-1935.

Barrett, E.C., and D.W. Martin, 1981. *The Use of Satellite Data in Rainfall Monitoring.* Academic Press.

Barrick, D.C., 1974. Wind dependence of quasi-specular microwave sea scatter. *IEEE Trans. Anten. Prop.*, AP-22, 135-136.

Bonbright, D.I., 1984. PODS SSM/I functional requirements (Version 1.0). JPL Pub. D-1793, Jet Propulsion Lab., Pasadena, CA, August 3.

Born, G.H., 1983. Error budget for GEOSAT altimeter height measurements. Center for Space Research Report of Sept. 14, 1983, Univ. of Texas at Austin, IN Rept. of Workshop Oceanography from GEOSAT, July 20-22, NORDA, NSTL Station, MS.

Cardone, V., T. Chester, and R. Lipes, 1983. Evaluation of SEASAT SMMR wind speed measurements. *J. Geophys. Res.*, 88, 1709-1726.

Carter, D.J.T., and P.G. Challenor, 1984. The impact of satellite altimeter data on wave research. ERS-1 Radar Altimeter Products Workshop, ESA, SP-221, 47-50.

CCCO, 1984. Ocean Observing System Development Programme, Committee on Climate Changes and the Ocean, IOC Tech. Series 27, IOC, Paris.

Challenor, P.G., and M.A. Srokosz, 1984. Extraction of wave period from altimeter data. ERS-1 Radar Altimeter Data Products Workshop, ESA.

Chang, H.D., P.H. Hwang, T.T. Wilheit, A.T.C. Chang, D.H. Staelin, and P.W. Rosenkranz, 1984. Monthly distributions of precipitable water from the Nimbus-7 SMMR data. *J. Geophys. Res.*, Special Issue.

Chelton, D., and P.J. McCabe, 1985. A review of satellite altimeter measurement of sea surface wind speed: With a proposed new algorithm. *J. Geophys. Res.*, 90 (in press).

Denman, K.L., and M. Miyake, 1973. Upper layer modifications at Ocean Station Papa: Observations and simulation. *J. Phys. Oceanogr.*, 3, 185-196.

Dobson, F.W., 1983. The Cage Experiment: Large-scale Oceanographic Experiments in the WCRP, Vol. II, WCRP Pub. Series 1, 419-435.

Fedor, L.S., and G.S. Brown, 1982. Wave height and wind speed measurements from the Seasat altimeter. *J. Geophys. Res.*, 87, 3254-3260.

Fissel, D.B., S. Pond, and M. Miyake, 1977. Computation of surface fluxes from climatological and synoptic data. *Mon. Wea. Rev.*, 105, 26-36.

Gloersen, P., and F.T. Barath, 1977. A scanning multichannel microwave radiometer for Nimbus-G and Seasat-A. *IEEE J. Oceanic Eng.*, OE-2, 172-178.

Grody, N.C., A. Gruber, and W.C. Shen, 1980. Atmospheric water content derived from the Nimbus 6 Scanning Microwave spectrometer over the tropical Pacific. *J. Appl. Meteor.*, 19, 986-996.

Guymer, T.H., *et al.*, 1985. A study of ERS-1 radar altimeter data processing requirements. Final Report, ESA-Contract 5681/83/NL/BI, ESA Publications, Noordwijk, Netherlands.

Hellerman, S., and M. Rosenstein, 1983. Normal monthly wind stress over the world ocean with error estimates. *J. Phys. Oceanogr.*, 13, 1093-1104.

Hobbs, P.V., 1978. Organization and structure of clouds and precipitation on the mesoscale and microscale in cyclonic storms. *Rev. Geophys. and Space Phys.*, 16, 741-755.

Hollinger, J.P., and R.C. Lo, 1983. SSM/I Project Summary Report. NRL Memorandum Rept. 5055, Naval Res. Lab., April.

Hollinger, J.P., and R.C. Lo, 1985. DMSP calibration validation plan for the Mission Sensor Microwave/Imager. Naval Res. Lab., March.

Hughes Aircraft Co., 1980. *Special Sensor Microwave/Imager Computer Program Product Specification*, Vol. II. CDRL No. 018A2, Hughes Aircraft Co., El Segundo, CA.

Hurlburt, H.E., and J.D. Thompson, 1984. Preliminary results from a numerical study of the New England Seamount Chain influence on the Gulf Stream. IN *Predictability of Fluid Motions*, G. Holloway and B.J. West, Eds., Amer. Inst. of Physics, New York, 489-504.

Hwang, P.H., and C.C. Fu, 1985. Analysis of Nimbus 7 SMMR retrieved wind speed (in preparation).

Jones, M.T., and A.R. Tabor, 1984. International banking of satellite and *in situ* wave data by MIAS. ERS-1 Radar Altimeter Data Products Workshop, ESA, SP-221, 91-98.

JPL, 1984. Satellite-derived sea surface temperature: Workshop I. JPL Pub. 84-5, Jet Propulsion Laboratory, Pasadena, CA, 76 pp.

Katsaros, K.B., P.K. Taylor, J.C. Alishouse, and R.J. Lipes, 1981. Quality of Seasat Scanning Multichannel Microwave Radiometer (SMMR) atmospheric water determinations. IN *Oceanography from Space*, Plenum Pub. Corp., 691-706.

Katsaros, K.B., and R.M. Lewis, 1984. Observing atmospheric water in storms with the Nimbus 7 Scanning Multichannel Microwave Radiometer. Paper Pres. at Internat. Un. of Radio Science Meeting, May 14-23, 1984, Shoresh, Israel.

Kilgus, C.C., and J.L. MacArthur, 1984. The Navy GEOSAT Mission Radar Altimeter Program. IN Conf. Proc. of Internat. Geosciences and Remote Sensing Symp., August 30, 1984 (to appear).

Liu, W.T., 1984. Estimation of latent heat flux with SEASAT SMMR, a case study in North Atlantic. IN *Large-scale Oceanographic Experiments and Satellites*, C. Gautier and M. Fieux, Eds., Reidel, Dordrecht, 205-221.

Liu, W.T., and P.P. Niiler, 1984. Determination of monthly mean humidity in the atmospheric surface layer over oceans from satellite data. *J. Phys. Oceanogr.*, 14, 1451-1457.

Luther, D.S., and D.E. Harrison, 1984. Observing long-period fluctuations of surface winds in the tropical Pacific: Initial results from island data. *Mon. Wea. Rev.*, 112 (in press).

McMurdie, L.A., and K.B. Katsaros, 1985. Atmospheric water distribution in a midlatitude cyclone observed by the Seasat Scanning Multichannel Microwave Radiometer. *Mon. Wea. Rev.* (in press).

McPhaden, M.J., 1982. Variability in the central equatorial Indian Ocean. Part II: Oceanic heat and turbulent energy balances. *J. Mar. Res.*, 40, 403-419.

Matejka, T.J., 1980. *Mesoscale Organization of Cloud Processes in Extratropical Cyclones.* Ph.D. Thesis, Dept. of Atmos. Sci., Univ. of Washington, Seattle, 361 pp.

Mitchell, J.L., 1984. The satellite altimeter as a platform for observation of the oceanic mesoscale. Proc. of IURS meeting, *Frontiers of Remote Sensing of the Oceans and Troposphere from Air and Space Platforms*, May 14-23, Tel Aviv, Israel (to appear).

Mitchell, J.L., Z.R. Hallock, and J.D. Thompson, 1985. The REX and the U.S. Navy GEOSAT. *Naval Res. Rev.* (in press).

NASA, 1982. *Scientific Opportunities Using Satellite Wind Stress Measurements over the Ocean.* Report of the Satellite Surface Stress Working Group, Nova Univ./NYIT Press, Ft. Lauderdale, FL, 153 pp.

NASA, 1984. Passive Microwave Remote Sensing for Sea Ice Research. Rept. of the NASA Science Working Group for the Special Sensor Microwave Imager (SSM/I), December.

Niiler, P.P., Ed., 1982. *Tropic Heat - A Study of the Tropical Pacific Upper Ocean Heat, Mass and Momentum Budgets.* Report, Oregon State Univ., Corvallis, OR, 30 pp.

Njoku, E.G., 1982. Passive microwave remote sensing of the earth from space: A review. *Proc., IEEE*, 70, 728-750.

Ramage, C.S., C.W. Adams, A.M. Hori, B.J. Kilonsky, and J.C. Sadler, 1980. *Meteorological Atlas of the 1972-73 El Niño.* UHMET 80-03, Univ. of Hawaii, Honolulu, HI, 101 pp.

Rao, M.S.V., W.V. Abbott III, and J.S. Theon, 1976. Satellite derived global oceanic rainfall atlas (1973 and 1974). NASA X-911-76-116, Goddard Space Flight Center, Greenbelt, MD.

Reed, R.K., 1983. Heat fluxes over the eastern tropical Pacific and aspects of the 1972 El Niño. *J. Geophys. Res.*, 14, 3627-3638.

Rhines, P.B., 1977. The dynamics of unsteady currents. IN *The Sea: Marine Modeling*, Vol. 6, E.D. Goldberg, I.N. McCave, J.J. O'Brien, and J.H. Steele, Eds., Wiley Interscience, New York, 189-318.

Richman, J., and C. Garrett, 1977. The transfer of energy and momentum by the wind to the surface mixed layer. *J. Phys. Oceanogr.*, 7, 876-881.

Schroeder, L.C., W.L. Grantham, J.L. Mitchell, and J.L. Sweet, 1982. SASS measurements of the KU-band radar signature of the ocean. *IEEE J. Oceanic Eng.*, OE-7, 3-14.

Spencer, R.W., 1985. An improved satellite passive 37 GHz method for measuring oceanic rainfall. *J. Clim. Appl. Meteor.* (Submitted).

Spencer, R.W., B.B. Hinton, and W.S. Olson, 1983. Nimbus 7 37 GHz radiances correlated with radar rain rates over the Gulf of Mexico. *J. Clim. Appl. Meteor.*, 22, 2095–2099.

Staelin, D.H., K.F. Kunzi, R.L. Pettyjohn, R.K.L. Poon, R.W. Wilcox, and J.W. Waters, 1976. Remote sensing of atmospheric water vapor and liquid water with the Nimbus 5 microwave spectrometer. *J. Appl. Meteor.*, 15, 1204–1214.

Stevenson, J.W., and P.P. Niiler, 1983. Upper ocean heat budget during the Hawaii-to-Tahiti Shuttle experiment. *J. Phys. Oceanogr.*, 13, 1894-1907.

Taylor, P.K., 1984. The determination of surface fluxes of heat and water by satellite microwave radiometry and *in situ* measurements. IN *Large-scale Oceanographic Experiments and Satellites*, C. Gautier and M. Fieux, Eds., Reidel, Dordrecht.

Taylor, P.K., T.H. Guymer, K.B. Katsaros, and R. G. Lipes, 1981a. Atmospheric water distributions determined by the Seasat Multichannel Microwave Radiometer. Paper Pres. at Oxford Global Water Symp., Aug. 10-15, 1981.

Taylor, P.K., K.B. Katsaros, and R. G. Lipes, 1981b. Determination by Seasat of atmospheric water and synoptic fronts. *Nature*, 294, 737-739.

Watts, D.R., and M. Wimbush, 1981. Sea surface height and thermocline depth variations measured from the sea floor. Proc. of the Internat. Symp. on Acoustic Remote Sensing of the Atmosphere and Oceans, June 22-25, 1981, Univ. of Calgary, Alberta, Canada.

WCRP, 1984a. Report of the Workshop on Interim Ocean Surface Wind Data Sets. World Climate Research Programme, Geneva, 43 pp.

WCRP, 1984b. Report of the Workshop on Sea Surface Temperature and Net Radiation Budget Products for Climate Research. World Climate Research Programme, Geneva (in press).

WCRP, 1984c. Report of the First Session of the JSC/CCCO WOCE Scientific Steering Group, WCP-69, World Climate Research Programme, Geneva.

WCRP, 1984d. Report of the Second Session of the JSC/CCCO WOCE Scientific Steering Group, WCP-81, World Climate Research Programme, Geneva.

Weare, B.C., and P.T. Strub, 1981. The significance of sampling biases on calculated monthly mean oceanic surface heat fluxes. *Tellus*, 33, 211-224.

Weare, B.C., P.T. Strub, and M.D. Samuel, 1980. *Marine Climate Atlas of the Tropical Pacific Ocean*, Univ. of California, Davis, CA, 147 pp.

Wentz, F.J., V.J. Cardone, and L.S. Fedor, 1982. Intercomparison of wind speeds inferred by the SASS, altimeter, and SMMR. *J. Geophys. Res.*, 87, 3378-3384.

Wentz, F.J., L.A. Mattox, and S. Peteherych, 1985. New algorithms for microwave measurements of ocean winds with application to SEASAT and SSM/I. *J. Geophys. Res.* (accepted).

Wilheit, T.T., and T.C. Chang, 1980. An algorithm for retrieval of ocean surface and atmospheric parameters from the observations of the Scanning Multichannel Microwave Radiometer (SMMR). *Radio Sci.*, 15, 525-544.

Wilheit, T.T., A.T.C. Chang, M.S.V. Rao, E.B. Rodgers, and J.S. Theon, 1977. A satellite technique for quantitatively mapping rainfall rates over the oceans. *J. Appl. Meteor.*, 16, 551-560.

Wilheit, T.T., A.T.C. Chang, J.L. King, E.B. Rodgers, R.A. Nieman, B.M. Krupp, A.S. Milman, J.S. Stratigos, and H. Siddalingaiah, 1982. Microwave radiometric observations near 19.35, 92 and 183 GHz of precipitation in Tropical Storm Cora. *J. Appl. Meteor.*, 21, 1137-1145.

Wylie, D.P., B.B. Hinton, and M.R. Howland, 1984. Wind stress on the tropical oceans during the year of FGGE. Univ. of Wisconsin Space Sci. and Engineering Center, Madison, WI.

APPENDIX A: RATIONAL RELATIONS BETWEEN MAGNITUDE AND DIRECTIONAL ERRORS IN VECTOR WIND AND FLUX FIELDS

Let s be the horizontal wind speed and let u be a unit vector in the direction of the wind. The vector wind is then represented by:

$$\hat{V} = s\hat{u} \tag{1}$$

By substituting the right side of (1), we can obtain the rates of change in the divergence (DIV) and curl (CURL) of the horizontal wind divergence induced by changes in wind speed and direction. To do this, let the wind direction (ψ) be defined such that:

$$\hat{u} = (cos\psi, sin\psi, 0) \tag{2}$$

Note that the definition of ψ adheres to mathematical rather than meteorological convention. Using (1) and (2), it is easily shown that

$$\partial DIV/\partial s = \nabla \cdot \hat{u} \tag{3}$$

$$\partial DIV/\partial \psi = -\nabla \times \vec{V} \tag{4}$$

$$\partial CURL/\partial s = \nabla \times \hat{u} \tag{5}$$

$$\partial CURL/\partial \psi = \nabla \cdot \vec{V} \tag{6}$$

Using the usual calculus of small errors, the root mean square error in DIV due to an error distribution of s having a root mean square deviation σ_s and zero mean is

$$\sigma_{DIV,s} = |\partial DIV/\partial s|\, \sigma_s \tag{7}$$

Analogous relations (8)–(10) apply as well, provided ψ is measured in radians:

$$\sigma_{DIV,\psi} = |\partial DIV/\partial \psi|\, \sigma_\psi \tag{8}$$

$$\sigma_{VOR,s} = |\partial VOR/\partial s|\, \sigma_s \tag{9}$$

$$\sigma_{VOR,\psi} = |\partial VOR/\partial \psi|\, \sigma_\psi \tag{10}$$

We can calculate the total variance in DIV and VOR from errors in both s and ψ, as in (11) and (12).

$$\sigma^2_{DIV} = \sigma^2_{DIV,\psi} + \sigma^2_{DIV,s} + r_{\psi,s}\, \sigma_{DIV,s}\, \sigma_{DIV,\psi} \tag{11}$$

$$\sigma^2_{VOR} = \sigma^2_{VOR,\psi} + \sigma_{VOR,s} + r_{\psi,s}\, \sigma_{VOR,s}\, \sigma_{DIV,\psi} \tag{12}$$

The r's in (11) and (12) are the correlation coefficients for the ψ- and s-errors. For present purposes, we consider only the cases for which r is zero, apply (3)–(12), and obtain:

$$\sigma^2_{DIV} = |\nabla \times \vec{V}|^2\, \sigma^2_\psi + |\nabla \cdot \hat{u}|^2\, \sigma^2_s \tag{13}$$

$$\sigma^2_{CURL} = |\nabla \cdot \vec{V}|^2 \sigma^2_\psi + |\nabla \times \hat{u}|^2 \sigma^2_s \tag{14}$$

Speed and direction measurements are compatible from the standpoint of DIV or $CURL$ if the errors induced in DIV or $CURL$ by speed and direction errors are of about the same magnitude. Under these conditions:

$$\sigma_\psi / \sigma_s \equiv |\nabla \cdot \hat{u}| \,/\, |\nabla \times \vec{V}| \tag{15}$$

$$\sigma_\psi / \sigma_s \equiv |\nabla \times \hat{u}| \,/\, |\nabla \cdot \vec{V}| \tag{16}$$

In real data and analysis systems, σ_ψ and σ_s depend on averaging time, desired spatial resolution, and other factors. For example, we found that for daily winds obtained by tracking low-level clouds extrapolated to the surface and ship observations, $\sigma_\psi \equiv 0.4$ radians and $\sigma_s \equiv 2.6\,\mathrm{ms}^{-1}$, typically. However, these vary from region to region and seasonally.

Preliminary comparisons among monthly gridded data suggest that σ_ψ and σ_s for monthly averaged data are about 0.2 radians and 1.1 ms^{-1}, respectively. For illustration purposes, the information in Tables A.1 and A.2 was developed for the global ocean strip between $\pm 20°$ lat. for January and July 1979.

The tables suggest that even on a monthly time scale, errors at an individual grid point are a large fraction of a typical (*i.e.*, rms) value of DIV and VOR. Something else is suggested — particularly by the January data. Even if no improvement were made in directional information, better speed data has a potential for reducing the total relative error. For example, if speed could be improved to the extent that its error contribution were the same as that of direction, the total error in January vorticity would drop from 39.8% to 24.0% - a 65% decrease. This requires a reduction of σ_s to about 0.5 ms^{-1}. Perhaps the measurements of speed (only) from satellite altimeters and microwave radiometers could significantly reduce speed errors.

Table A.1: Mean Square Magnitude of *DIV* and *VOR* and the Contributions to Errors in *DIV* and *VOR* for Unit Errors in Speed and Direction. (All entries in the first 3 lines should be multiplied by 10^{-7}. Units of angle are radians; speed has units of ms^{-1}. All data are for 1979.)

	January		July	
	DIV	VOR	DIV	VOR
Magnitude (rms)	33.8	39.7	27.1	41.8
Error per unit directional error	39.7	33.8	41.8	27.1
Error per unit speed error	11.4	13.0	7.7	7.0
Number in sample	733	733	727	727

Table A.2: Errors in *DIV* and *VOR* of the Wind due to Errors in Speed and Direction. (Errors are in units of 10^{-7}. The assumed error in direction was 0.2 radians; for speed, a 1.1 ms^{-1} error was assumed. Data are for 1979 only.)

	January		July	
	DIV	*VOR*	*DIV*	*VOR*
Error due to direction	7.94	6.76	8.36	5.42
Relative error due to direction (%)	23.5	17.0	30.8	13.0
Error due to speed	12.5	14.3	8.47	7.70
Relative error due to speed (%)	37.1	36.0	31.3	18.4
Total relative error (rms; %)	43.9	39.8	43.8	22.5

APPENDIX B: GLOSSARY OF TERMS

ALT	Altimeter radar
BAPTA	Bearing and Power Transfer Assembly
crossovers	ground track intersections
DMA	Defense Mapping Agency
DMSP	Defense Meteorological Satellite Program
DOD	Department of Defense
EDR	Environmental Data Record
ENSO	El Niño/Southern Oscillation
EPOCS	Equatorial Pacific Ocean Climate Studies
ERM	Exact Repeat Mission
ERS-1	proposed oceanographic altimeter system
FASINEX	Frontal Air-Sea Interaction Experiment
FNOC	Fleet Numerical Oceanography Center
GEO	Geostationary satellite
GEOS	Geodynamic Earth Observation System
GEOSAT	Geodetic Satellite
GPS	Global Positioning System
IES/PG	Inverted Echo Sounder/Pressure Gauge
IOC	Intergovernmental Oceanographic Commission
IODE	International Oceanographic Data Exchange
JASIN	Joint Air-Sea Interaction Experiment
LEO	Low Earth Orbiting satellite
MIAS	Marine Information and Advisory Service
NASA	National Aeronautics and Space Administration
NDBO	National Data Buoy Office
NESDIS	National Environmental Satellite, Data, and Information Service
NGS	National Geodetic Survey
NOAA	National Oceanic and Atmospheric Administration
NORDA	Naval Ocean Research and Development Activity
NRCS	Normalized Radar Cross Section
N-ROSS	Navy Remote Ocean Sensing System
NSSA	Navy Space Systems Activity
ONR	Office of Naval Research
PODS	Pilot Ocean Data System
REX	Regional Energetics Experiment
RSS	Remote Sensing Systems
SASS	SEASAT Scatterometer
SAWG	Sea-Ice Algorithm Working Group

SDR	Sensor Data Record
SEASAT	Sea Satellite
SMMR	Scanning Multichannel Microwave Radiometer
SSM/I	Special Sensor Microwave/Imager
T_a	Antenna temperature
TDR	Temperature Data Record
TOGA	Tropical Ocean and Global Atmosphere
TOPEX	Ocean Topography Experiment
TWTA	Traveling Wave Tube Amplifier
WCRP	World Climate Research Program
WMO	World Meteorological Organization
WOCE	World Ocean Circulation Experiment

End of Document